Rictor/mTORC2 deficiency enhances keratinocyte stress tolerance via mitohormesis.

Rictor/mTORC2 deficiency enhances keratinocyte stress tolerance via mitohormesis.

Beatrice Tassone[1], Stefania Saoncella[1], Francesco Neri[1,3], Ugo Ala[1], Davide Brusa[3], Mark A. Magnuson[5], Paolo Provero[1,4], Salvatore Oliviero[2,3], Chiara Riganti[6] and Enzo Calautti[1,7].

[1]Department of Molecular Biotechnology and Health Sciences, University of Turin, Turin, Italy

[2]Department of Life Sciences and System Biology, University of Turin, Turin, Italy;

[3]Human Genetics Foundation, HuGeF, Turin, Italy

[4]Center for Translational Genomics and Bioinformatics, San Raffaele Scientific Institute, Milan, Italy

[5]Department of Molecular Physiology and Biophysics, Vanderbilt University School of Medicine, Nashville, TN, USA

[6]Department of Oncology, University of Turin, Turin, Italy

[7]Corresponding author:

Enzo Calautti, M.D., Ph.D, Via Nizza 52, 10126 Turin Italy; Telephone: +39-011-6706411; Fax: +39-011-6706432; e-mail: vincenzo.calautti@unito.it

Abstract

How metabolic pathways required for epidermal tissue growth and remodeling influence the ability of keratinocytes to survive stressful conditions is still largely unknown. The mechanistic target of rapamycin complex 2 (mTORC2) regulates growth and metabolism of several tissues, but its functions in epidermal cells are poorly defined. Rictor is an adaptor protein essential for mTORC2 activity. To explore the roles of mTORC2 in the epidermis, we have conditionally deleted *rictor* in mice via K14-Cre-mediated homologous recombination and found that its deficiency causes moderate tissue hypoplasia, reduced keratinocyte proliferation and an attenuated hyperplastic response to TPA. Noteworthy, rictor-deficient keratinocytes displayed increased lifespan, protection from senescence, and enhanced tolerance to cellular stressors such as growth factors deprivation, epirubicin and X-ray *in vitro* and radioresistance *in vivo*. Rictor-deficient keratinocytes exhibited changes in global gene expression profiles consistent with metabolic alterations and enhanced stress tolerance, a shift in cell catabolic processes from glycids and lipids to glutamine consumption and increased production of mitochondrial reactive oxygen species (ROS). Mechanistically, the resiliency of rictor-deficient epidermal relies on these ROS increases, indicating stress resistance via mitohormesis. Thus, our findings reveal a new link between metabolic changes and stress adaptation of keratinocytes centered on mTORC2 activity, with potential implications in skin aging and therapeutic resistance of epithelial tumors.

Introduction

Adaptation to stressful conditions is key for organisms evolution and the epidermis contributes to this function providing a barrier against physical and chemical injuries, dehydration and pathogens infection (1).

From yeast to mammals, stress tolerance and lifespan extension are favored by low nutrients conditions leading to increased metabolic rates (2, 3). Caloric restriction, low glucose intake and inhibition of the insulin/IGF pathway parallel with extended lifespan and mild increases of reactive oxygen species (ROS) (4, 5). Albeit traditionally considered as purely harmful, ROS are physiological regulators of stress response mechanisms that prevent cellular damage (3, 6 and references therein). Mitohormesis is a process initiated by moderate increases of mitochondrial ROS, which enhance resistance to stressors by engaging programs of cell protection (3 and references therein). Although molecular pathways including Akt, p53, Nrf2, NFκB and AP1 regulate the epidermal responses to oxidative damage, UV and X-ray radiations and chemotherapic drugs (7-9), whether mitohormesis plays a role in keratinocyte stress adaptation is unknown.

The mechanistic target of rapamycin (mTOR), an evolutionarily conserved serine/threonine protein kinase, is a signaling hub integrating cell growth, metabolism and energy stress responses (10). mTOR signaling is activated by extracellular cues such as nutrients and growth factors, and favors cellular and organismal growth by stimulating biosynthesis of macromolecules. mTOR inhibition causes lifespan extension via mitohormesis in yeast (11), and prevents energy expenditure by promoting autophagic recycling of cellular components (12). mTOR kinase is the catalytic subunit of two signaling complexes, mTOR Complex1 (mTORC1) and mTOR Complex2 (mTORC2) (13). While most mTOR biological functions have been attributed to mTORC1 (14), mTORC2 regulates AGC family protein kinases such as Akt and PKC isoforms necessarily adjuvated by the evolutionarily conserved adaptor protein Rictor (13). By phosphorylating Akt proteins at a regulatory

residue (Ser473 in Akt1) in response to growth factors, mTORC2 promotes maximal Akt kinase activity and cell survival in mammals, and regulates actin cytoskeleton via PKC signaling (15, 16).

In mammals, germline ablation of *rictor* is incompatible with development (17). While tissue-specific embryonic ablation of *rictor* interferes with morphogenesis in the vascular endothelium and nervous systems (18, 19), its deletion in skeletal muscle, adipose tissue and liver impairs lipogenesis and glucose metabolism (20-22).

Here we show that rictor conditional ablation during epidermal development causes tissue hypoplasia in the newborn mice paralleled with attenuated keratinocyte proliferation rates. Importantly, rictor/mTORC2 deficiency in keratinocytes causes delayed senescence, enhanced resistance to cellular stressors, and a shift of catabolic functions towards glutaminolysis, elevated mitochondrial activity and ROS production. These ROS increases play a mitohormetic role, being crucial for the resiliency of rictor-deficient keratinocytes. Thus, our work implicates rictor/mTORC2 as a novel signaling node integrating epidermal metabolism with stress adaptation.

Results

Rictor/mTORC2 disruption in murine epidermis leads to tissue hypoplasia in newborn mice

To conditionally delete *rictor* in the epidermis, mice carrying a *rictor* allele in which exon 3 is flanked by two loxP sites (17) were bred with mice expressing Cre recombinase under the control of the *keratin 14* (K14) promoter (23) (Fig.1a). Newborn mice with K14-Cre-mediated homozygous deletion of rictor (E-RiKO mice) displayed undetectable levels of rictor protein in the epidermis while the mTORC1-specific raptor levels were unchanged (Fig.1b) compared to control (CT) mice. E-RiKO mice were born at the expected Mendelian rate and did not show obvious epidermal or hair follicle abnormalities from birth until 1 year of age (not shown). Immunoblotting analysis confirmed ablation of rictor in E-RiKO keratinocytes paralleled by nearly-abrogated phosphorylation of Ser473 Akt in response to growth factors, whereas phosphorylation of Thr308 Akt was preserved. Keratinocytes, like other cell types, exhibited reduced total Akt and PKCα levels following rictor ablation (Fig.1c) (13) without significant alterations of mTORC1 signaling or Akt targets phosphorylation, except for attenuated phosphorylation of FoxO1 and -3 (24) (Fig.S1a), thereby displaying features typical of mTORC2 disruption.

Compared to CTs, E-RiKO epidermis was stratified but thinner (Fig.1d) in newborn animals. Such hypoplasia was unlikely the result of cell death since we did not detect TUNEL- or cleaved caspase-3 positivity in the epidermis (not shown). In contrast, positivity for the PCNA proliferative marker was reduced in E-RiKO mice (Fig.1e). p63 and loricrin, used as readouts of progenitor and differentiated keratinocytes, respectively, were expressed with proper spatial tissue distribution albeit at lower levels in mutant mice (Fig.S1b-c), suggesting that hypoplasia reflects impaired cell growth affecting the cellularity of different epidermal compartments. Instead, the thickness of adult murine epidermis, composed by only two-three cellular layers, was comparable between CT and

mutant mice (Fig.1f). TPA treatment of adult epidermis induces rapid keratinocyte proliferation resulting in hyperplasia by 48h (25). 7-week old E-RiKO mice displayed attenuated epidermal thickening upon TPA exposure (Fig.1f), paralleled by a decreased BrdU incorporation (Fig.1g). Thus, mTORC2 deficiency restrains growth and hyperplasia of the epidermis in part by attenuating mitogenic responses.

Rictor/mTORC2 deficiency impairs keratinocytes proliferation and delays senescence *in vitro*

We compared primary keratinocytes derived from CT or E-RiKO newborn littermates under proliferating conditions (low calcium medium; LCM) and monitored until CT cells reached senescence. Consistent with the hypoplastic phenotype, the number of keratinocytes isolated from E-RiKO epidermis was reduced relative to CT counterparts (Fig.2a). E-RiKO keratinocytes displayed attenuated growth rates (Fig.2b), decreased percentages of $BrdU^+$ cells (Figs.2c; S2a), reduced cell density (Fig.2d), decreased S-phase and a proportional increase in the G0/G1 phase (Fig.S2b). Notably, whereas CT keratinocytes acquired a senescent-like morphology, E-RiKO cells exhibited proliferative appearance until at least 20-25 days from plating (Fig.2d) and lower levels of p16, p19 and p53 senescence markers (Fig.2e) and β-galactosidase activity (Fig.2f). Moreover, albeit LCM culture conditions are unfavorable for spontaneous keratinocyte immortalization (26), E-RiKO cultures became immortalized with 100% efficiency as compared to ~18% of CTs (Fig.S2c-e).

Rictor-deficient keratinocytes are protected from death induced by multiple cellular stressors

Several molecular determinants of cell senescence are also implicated in cell death. Upon growth factors deprivation, E-RiKO cells displayed reduced morphological death signs

(Fig.S3a), delayed/attenuated caspase-3 cleavage (Cl-Casp3) (Fig.3a) and decreased cell death by AnnexinV/DAPI analysis (Fig.3b). By comparing the responses to epirubicin, an anticancer drug that induces cell death via DNA damage and oxidative stress (27), the majority of CT cells detached after 15h of treatment, whereas many E-RiKO cells seemed unaffected (Fig.S3a) and displayed lower Cl-casp3 levels (Fig.3c) and reduced death (Fig.3d). Since the S-phase of the cell cycle renders cells vulnerable to epirubicin, we verified if the reduced sensitivity of E-RiKO keratinocytes reflected their reduced division rates by exposing cells to the drug under comparable growth arrested conditions (Fig.3e). Even in this case, E-RiKO cells displayed lower Cl-casp3 levels (Fig.3f), suggesting that their resiliency does not simply depend on attenuated proliferation.

We next evaluated the effects of different X-ray doses. E-RiKO cells retained higher clonogenic ability upon X-ray exposure (Fig.3g), confirming enhanced stress tolerance. Keratinocytes are highly refractory to X-ray-induced apoptosis (28); hence, we evaluated cell death by AnnexinV/DAPI analysis after one 60Gy dose, which induces ~30% of cell death in CT keratinocytes. E-RiKO cells had a ~25% reduction in cell death (Fig.3h). Irradiated E-RiKO cells showed attenuated Cl-casp3 (Fig.S3d), and displayed a reduction in both senescence (Fig.S3e, S3f) and growth arrest in response to X-ray (Fig.S3g). Mutant keratinocytes exhibited reduced H2AX phosphorylation (γH2AX) suggestive of lower DNA damage (Fig.S3d), and decreased Chk1 and Chk2 levels (Fig.S3d) similarly to cancer cells subjected to rictor or mTOR ablation (51). Interestingly, in CT cells, Ser473 Akt phosphorylation decreased early on after X-ray exposure. In contrast, treatment of E-RiKO and CT keratinocytes with the DNA-damaging agent cisplatin did not reveal significant differences in morphology, sensitivity to apoptosis, levels of Cl-casp3 and γH2AX, and in CT cells Akt Ser473 phosphorylation was not reduced at early times (Fig.S3a-c). Thus, E-RiKO keratinocytes are not resistant to death *per se* and retain functional apoptotic machinery.

To verify whether rictor deficiency protects keratinocytes from X-ray-induced cell death *in vivo*, we analyzed the skins of irradiated E-RiKO and CT littermates by TUNEL assay. Consistent with previous reports, positivity to the staining was minimal in the interfollicular epidermis (29), and $TUNEL^+$ keratinocytes were confined within the hair follicle matrix (30) (Fig.3i). Notably, E-RiKO mice displayed a significant decrease in $TUNEL^+$ cells compared to CT littermates (Fig.3j).

Gene expression profiles of rictor-deficient keratinocytes indicate metabolic alterations under basal conditions and upon X-ray exposure

To identify specific genes and pathways involved in the enhanced stress tolerance of E-RiKO keratinocytes, we performed a RNA-seq transcriptome analysis by comparing mutant and CT cells under basal growing conditions, and at different times after X-ray exposure (Table S1). Under basal conditions, 589 genes were differentially regulated between E-RiKO and CT cells, i.e. 336 downregulated and 253 upregulated genes in the former (Fig.4a; Tables S2-3). Gene Ontology (GO) enrichments were considered significant with a nominal P value less than 10^{-3} with Fisher exact test. Rictor deficiency was associated with significant enrichment of genes involved in lipid metabolism, keratinocyte differentiation, oxidation-reduction process, lipid catabolic process and lipid biosynthetic process among downregulated genes, and genes involved in cell motility, signal transduction, inflammatory response, response to stress and defense response among upregulated genes (Fig.4b). The complete GO analysis is provided in Tables S4-5. By evaluating the number of modulated genes after 1h of X-ray exposure versus basal conditions, E-RiKO keratinocytes displayed a dramatically reduced response to the treatment (i.e. 94 versus 794 genes), while after 24h the differences between genotypes were attenuated (Fig.4c).

Based both on these results and the greater stress tolerance of mutant cells, we hypothesized that genes modulated in CT cells following treatment might be similarly up- or downregulated in E-RiKO under basal conditions. To this aim, we compared differentially expressed genes (DEGs) in CT cells under X-ray treated (1h) versus basal conditions, with DEGs in E-RiKO versus CT cells under basal conditions (Fig.4d). Notably, we found a highly significant 27.5% genes overlap (P=5.44E-57), corresponding to 161 DEGs (62% downregulated and 38% upregulated). The majority of these genes were expressed at similar levels in basal E-RiKO cells and X-ray exposed CT cells (Tables S1, S6-7). GO analysis of this subgroup of genes revealed an enrichment in lipid metabolic process, lipid catabolic process, response to hypoxia and lipid biosynthetic process in the downregulated class whereas few GO survived in the upregulated class at this stringency, among which regulation of epithelial cell proliferation and response to glucose (Fig.4e; Tables S6-7). These data suggest that rictor deficiency alters the metabolic functions of keratinocytes under basal conditions, and because several metabolic genes that were rapidly turned down in CT cells in response to X-ray were basally downregulated in E-RiKO cells, this suggests a link between metabolic changes and stress adaptation.

Rictor deficiency in keratinocytes promotes metabolic rewiring and ROS production

ROS contribute to cell death mechanisms triggered by growth factors deprivation, epirubicin and X-ray, while cisplatin, to which E-RiKO cells are sensitive, promotes cell death primarily via direct DNA damage independently of ROS (31). To our surprise, we detected higher basal levels of ROS (~1.7 fold) in E-RiKO keratinocytes relative to CT counterparts (Fig.5a), while 24h after X-ray exposure CT cells displayed a more robust increase (~2.9 fold vs 1.2 fold) (Fig.S3f). Mitochondrial ROS were also higher in E-RiKO cells (Fig.5b-5c). By contrast, the activity of aldose reductase, a source of cytosolic ROS (32), was reduced of 20% in E-RiKO (Fig.5d) while NADPH oxidase activity, which also

generates cytosolic ROS, was similar (Fig.5e). The electron transport chain (Fig.5f) and the amounts of mitochondrial ATP (Fig.5g) were instead increased, suggesting that rictor-deficiency promotes increases of mitochondrial ROS and respiration.

Consistent with mTORC2 deficiency being coupled with defective lipogenesis (21, 22), E-RiKO cells had reduced triglycerides levels (Fig.5i), as suggested by GO analysis. We then analyzed the activity of catabolic pathways that may impinge on ROS production by fueling mitochondrial oxidative phosphorylation. Fatty acid β-oxidation was reduced to ~60% of CT values in E-RiKO cells (Fig.5h), in agreement with RNA-seq data (Fig.4b). Moreover, E-RiKO cells showed decreased glucose uptake and glycolysis (Fig.5j-l). The glutaminolysis energetic pathway provides carbon source alternative to lipids and glycids, nitrogen for nucleotide biosynthesis and NADPH for redox maintenance (33). E-RiKO keratinocytes showed increased activity of both glutaminase (2.3 fold) and glutamic dehydrogenase (1.5 fold), which catalyze the first and the second step of glutaminolysis, respectively, although we did not detect alterations in their mRNA and/or protein levels (Fig.5m-n, Table S1 and data not shown). Moreover, in both L-[^{14}C]-glutamine- or L-[^{14}C]-glutamate-labeled cells the flux through the Tricarboxylic acid (TCA) cycle was higher in rictor-deficient keratinocytes, and was reduced by the glutaminase inhibitor BPTES ((1Z,1'Z)-N',N''-(5,5'-(thiobis(ethane-2,1-diyil))bis(1,3,4-thiadiazole-5,2-diyil))bis(2-phenylacetimidic acid)) (Fig.S4a), in L-[^{14}C]-glutamine-treated cells but not in L-[^{14}C]-glutamate-labeled cells (Fig.5o-p), suggesting that TCA cycle was strongly fueled by the glutaminolytic anaplerotic reaction in E-RiKO cells.

Since the production of glutamate represents the first obligatory step in glutamine catabolism, the ratio between intracellular L-glutamate versus L-glutamine – after pulsing cells with L-[^{14}C]-glutamine - was used as readout of glutamine consumption: while glutamine uptake was similar between genotypes, in E-RiKO cells both the production of glutamate and the ratio between L-glutamate and L-glutamine was more elevated (Fig.5q-

239 s). Thus, rictor deficiency promotes keratinocyte metabolic reprogramming, diverting the
240 catabolism from lipids and glycids to glutamine consumption.
241 To verify whether E-RiKO cells possessed higher antioxidant capacity, we measured the
242 activities of the main anti-oxidant enzymes, cytosolic- and mitochondrial superoxide
243 dismutases (SODs) and catalase. Mitochondrial SOD activity was more than doubled in E-
244 RiKO cells compared to CTs (Fig.5t-v), whereas cytoplasmic SOD and catalase activities
245 did not differ significantly. Because the levels of catalase, SOD1 and SOD2 proteins,
246 which account for SOD activities in cytosol and mitochondria, respectively, were
247 unchanged (Fig.S4b, Table S1 and data not shown), the enhanced mitochondrial SOD
248 activity of E-RiKO cells may rely on post-translational modifications of SOD2.
249
250 **Rictor-deficient keratinocytes are sensitized to epirubicin-induced cell death by**
251 **antioxidant treatment and glutaminase inhibition**
252 To define whether the increased ROS of E-RiKO cells are responsible for their stress
253 resistant phenotype, we treated E-RiKO and CT keratinocytes with epirubicin in the
254 presence of ROS scavenger N-Acetyl Cysteine (NAC) at a concentration able to lower
255 total- and mitochondrial ROS in E-RiKO cells to levels close to untreated CT cells (Fig.6a-
256 b). Without NAC, E-RiKO keratinocytes resulted more resistant to apoptosis in response to
257 epirubicin, whereas NAC-treated E-RiKO keratinocytes displayed Cl-casp3 and
258 AnnexinV/DAPI profiles close to those of CT cells unexposed to NAC (Fig.6c-d), indicating
259 that this compound sensitizes E-RiKO cells to epirubicin-induced apoptosis. This was
260 apparently in contrast to findings reporting that cells are protected from epirubicin-induced
261 death by a NAC pretreatment up to 24h (34). Under these conditions we could detect a
262 significant reduction of Cl-casp3 (Fig.S5a) in CT keratinocytes, but we were unable to
263 restore normal ROS levels in E-RiKO cells (Fig.S5b). These data suggest that prolonged
264 versus transient ROS scavenging has different effects on the stress tolerance of normal

keratinocytes. Also Trolox (6-hydroxy-2,5,7,8-tetramethylchroman-2-carboxylic acid), a distinct antioxidant compound, restored normal ROS levels in E-RiKO cells and increased Cl-casp3 levels in response to epirubicin (Fig.S5c-d).

NAC exposure of CT and E-RiKO cells did not affect other metabolic parameters (Fig.S5e), apart from the decrease of mitochondrial SOD activity in mutant cells to levels similar to untreated CT cells.

These data suggest that the activity of NAC is primarily due to its antioxidant capacity, and that the increased ROS are not the inducers of the metabolic changes produced by rictor deficiency but rather their consequence.

The increased ROS of E-RiKO cells may depend on increased glutaminolytic activity. Consistent with this hypothesis, BPTES effectively reduced glutaminase activity in both genotypes and restored in E-RiKO treated cells ROS levels similar to CT cells (Fig.6e-f), indicating glutaminase as a major determinant of ROS increases. Importantly, sustained glutaminase inhibition also phenocopied the effects of NAC in E-RiKO cells, as it increased both Cl-casp3 levels and cell death in response to epirubicin (Fig.6g-h). Thus, both the reestablishment of normal ROS levels and the inhibition of their principal metabolic source sensitize E-RiKO cells to stressors to which they are typically resistant. ROS scavenging by NAC also attenuated features of E-RiKO cells beyond stress response such as their decreased BrdU uptake (Fig.S5f) and protection from senescence (Fig.S5g), suggesting the involvement of ROS also in these phenotypes.

The epidermal metabolic, molecular and stress-response phenotypes of E-RiKO mice indicate a critical role of ROS in stress protection

To determine whether metabolic alterations observed in cultured E-RiKO keratinocytes were present in the epidermis of mutant mice *in vivo*, we compared several metabolic parameters in fresh epidermal extracts obtained from CT and E-RiKO mice (Fig.7a).

Relative to CT mice, total- and mitochondrial ROS, electron transport chain activity, ATP content, glutaminase and glutamic dehydrogenase activities were all more elevated in mutant mice, while lipid β-oxidation and hexokinase activities were reduced, reflecting closely the findings on cultured cells.

We next analyzed in CT and E-RiKO epidermis the expression of a sample of DEGs between CT and E-RiKO keratinocytes emerged from RNA-seq analysis. As shown in Fig.7b, the levels of Gadd45α, –β and -γ, Glul and Il1-α genes, involved in DNA repair, glutamine metabolism and inflammation, upregulated in E-RiKO cells (Table S1), were also higher in the mutant epidermis whereas the levels of Acsl1, Faah and Fabp4, involved in lipid metabolism, were decreased.

To determine whether NAC treatment could sensitize E-RiKO hair follicle keratinocytes to X-ray-induced death *in vivo*, we established a NAC treatment regimen restoring ROS levels in mutant mice to levels close to CTs (Fig.7d). As shown in Fig.7c-e, NAC treated E-RiKO mice exhibited a statistically significant increase in the number of $TUNEL^+$ cells in the hair follicle matrix upon irradiation, suggesting that restoring normal ROS levels in E-RiKO mice sensitizes hair follicle keratinocytes to X-ray induced cell death *in vivo.* Moreover, NAC slightly increased the number of $TUNEL^+$ CT cells (Fig.7e and data not shown). Thus, many aspects of the metabolic, molecular and stress response phenotypes described in primary keratinocytes derived from E-RiKO mice are recapitulated in their intact skin epithelia *in vivo.*

Discussion

Our study reveals for the first time that mTORC2 couples metabolic changes with stress adaptation in mammalian cells. The resiliency of rictor-deficient keratinocytes to starvation, epirubicin and X-ray *in vitro* and their radioresistance *in vivo* was somewhat surprising, considering the pro-survival role of mTORC2 in mammals (15). However, mTORC2 deficiency does not render keratinocytes resistant to cell death *per se* but likely enhances their ability to cope with oxidative stress since these cellular stressors share ROS production among their death effector mechanisms (27). Because in control keratinocytes Akt Ser473 phosphorylation decreases early on upon X-ray (but not cisplatin) treatment, attenuation of mTORC2 activity may be intrinsic to the keratinocyte response to specific stressors.

Our findings in mammalian cells have intriguing analogies in Drosophila, where rictor deficiency promotes resistance and tolerance to pathogens infection under low glucose (35), suggesting a conserved role of mTORC2 in integrating metabolic cues and stress adaptation. Since the mTORC2/Akt axis positively regulates glucose uptake and glycolysis in several tissues (22, 36), the stress-resistant phenotype of E-RiKO cells may result from their adaptation to impaired glucose consumption and rewiring towards glutaminolysis. The increased glutamine consumption of E-RiKO keratinocytes is associated with increased activity of glutaminolytic enzymes without changes in their protein or mRNA levels suggesting that rictor deficiency may affects these enzymes via post-translational modifications or by changing the concentration of allosteric modulations, as it occurs upon mTORC2 disruption (37). Additionally, rictor loss may impinge on Foxo transcription factors in linking metabolic changes with stress resistance. Foxo3 regulates glutamine metabolism via Glul expression (38); Glul is overexpressed in E-RiKO cells that also have reduced Foxos phosphorylation, and among stress protective genes overexpressed in E-RiKO cells are the Foxo targets Gadd45 isoforms (39).

Mitochondrial SOD enzymatic activity, playing a pivotal role in radioprotection (40), is elevated in E-RiKO cells, and decreases upon NAC treatment. Active SOD2 is stabilized by oxidative cross-linking, favoring radioresistance of cells exposed to conditioning doses of oxidative stress (41). Enhanced SOD2 expression accounts for radioresistance of rapamycin-treated oral keratinocytes (40), and SOD2 activity can be regulated post-translationally in response to ROS levels (41). Therefore, changes in SOD2 activity likely favor stress adaptation in rictor-deficient keratinocytes, albeit the underlying mechanisms remain undefined.

The increased ROS levels of E-RiKO keratinocytes, instead of being harmful, emerged as key determinants of their stress-resistant phenotype. Therefore, the behavior of rictor-deficient keratinocytes fits well with the concept of mitohormesis, implicating mTORC2 in radioresistance, and possibly, skin aging. Hormetic behaviors occur in several cell lineages including keratinocytes, and mild level of X-ray render cells more resistant to a subsequent damage (42).

Our findings overall suggest that the switch of keratinocyte catabolism towards glutaminolysis provides fuel for mitochondrial respiration and ROS production, which, directly or indirectly, induces expression of stress resistance genes.

Rictor deficiency was associated with decreased cell division (18, 43) and the attenuated proliferation of E-RiKO keratinocytes likely underlies the epidermal hypoplasia of mutant mice, albeit we cannot rule out subtle defects in differentiation or cytoskeleton dynamics. Adult E-RiKO mice epidermis does not display hypoplasia or impaired proliferation unless challenged with a mitogen like TPA; in growth factor-rich conditions E-RiKO keratinocytes also exhibit reduced division rates, suggesting that mTORC2 loss affects proliferation upon robust mitogenic inputs. The attenuated hyperplastic response to one single TPA dose reported here differs from the normal hyperplastic response to multiple TPA doses described in mice subjected to epidermal-specific, inducible rictor ablation during

363 adulthood (44). Metabolic alterations coupled with enhanced stress tolerance likely
364 contribute to the delayed senescence and lifespan extension of rictor-deficient
365 keratinocytes, in keeping with similar reports on fibroblasts (45). Since hyperactive DNA
366 replication forks promote senescence, the spontaneous immortalization of E-RiKO
367 keratinocytes may result from senescence bypass favored by metabolic reprogramming,
368 mitohormesis and reduced proliferation rates. Since sustained exposure of E-RiKO
369 keratinocytes to NAC enhances BrdU uptake and favors senescence in the absence of
370 exogenous stressors, ROS elevations may contribute to the proliferative and senescence
371 phenotypes of mutant cells.
372 Mitohormesis may represent a point of convergence of mTORC1 and mTORC2 activities
373 across species. In fact, mTORC1 inhibition extends yeast chronological lifespan (11); the
374 mTOR inhibitor rapamycin extends lifespan in C.Elegans and mice (46, 47) and prolonged
375 rapamycin exposure also inhibits mTORC2 (47, 48); rictor deficiency in yeast was linked to
376 increased ROS levels (49), and in C.Elegans, *rictor* mutations extend lifespan in a nutrient-
377 dependent manner (50).
378 The choice between cell survival and death upon mTORC2 disruption may be highly
379 context-dependent. Rictor/mTORC2 deficiency sensitizes fibroblasts to UVB-induced
380 apoptosis (51), but the mechanisms regulating DNA repair and apoptosis differ between
381 keratinocytes and fibroblasts (52), possibly accounting for this apparent discrepancy.
382 Additionally, in breast cancer cells, mTORC2 loss favors cell cycle progression and
383 apoptosis by lowering Chk1 activity and increasing vulnerability to DNA damage (51); in E-
384 RiKO cells Chk1 attenuation coincides with lower DNA damage in response to X-ray, but
385 not cisplatin. mTOR inhibition can inhibit or enhance chemotherapy-induced cancer cell
386 death in oncological settings (53); if mTOR inhibition enhances stress tolerance via
387 mitohormesis, this could partly explain the limited efficacy of mTOR inhibitors in this
388 context (54). mTORC2 disruption inhibits tumor formation/progression in many tissues

389 including the epidermis (44), but caution should be taken in therapeutic settings since
390 mTOR inhibition may also promote chemo- or radioresistance. Our work suggests
391 however that combination of mTOR inhibitors with anti-oxidants may help sensitizing
392 tumors that would be otherwise resistant to chemo/radio-therapy.
393

Materials and Methods

Mice generation and Genotyping

Generation of rictor conditional knock-out mice in the epidermis (E-RiKO) was obtained by crossing Rictor flox/flox mice (CT) described in (17) with K14-Cre transgenic mice (23). Mice were studied on a C57BL/6J background. Genetic screening was performed by PCR using DNA extracted from tail biopsies.

The primer used for genotyping were as follows:

- Rictor flox Forward, 5' – ACTGAATATGTTCATGGTTGTG
- Rictor flox Reverse, 5' – GACACTGGATTACAGTGGCTTG
- K14-cre Forward, 5' – AGGGATCTGATCGGGAGTTG
- K14-cre Reverse, 5' – CTTGCGAACCTCATCACTCG

Mice were maintained under temperature and humidity controlled conditions and were given food and water *ad libitum*. Procedures were conducted in conformity with national and international laws and policies as approved by the University of Turin Ethical Committee.

Cell Cultures and Chemicals

MPKs were isolated from pools of 3-day-old (P3) mice and cultured in Low Calcium Medium (LCM, 50μM $CaCl_2$ supplemented with 4% Chelex-treated Bovine Serum and EGF). Cultures were ~95% pure and contained traces of malanocytes and Langerhans' cells. MPKs cultures were obtained from at least 5 mice/genotype and, unless otherwise specified, all experiments were repeated on at least 3 independent cultures.

Note that MPKs cultured in LCM keep proliferating even at confluency because they are preserved from contact inhibition, and dividing cells replace the differentiated ones that lift from the adherent cell monolayer.

Starvation was performed culturing MPKs in Serum and EGF-free LCM, except for kinetic analysis of BrdU incorporation, in which cells were starved in 0.1% serum.

Cells fed with LCM (or starved) were treated with the following chemicals: Epirubicin, Cisplatin and NAC (Sigma-Aldrich, St. Louis, MO, USA), Trolox (Santa Cruz Biotechnology, Dallas, TX, USA) and BPTES (Selleckchem, Houston, TX, USA).

NAC treatments were performed by adding the compound into fresh LCM every 24h. To evaluate proliferation, MPKs were incubated with 5-bromo-2”-deoxy-uridine (BrdU, Invitrogen, Waltham, MA, USA) 3h prior the end of the experiment (10μg/ml) and then fixed in PFA 4%.

Colony-forming efficiency (CFE) assays were performed as described (55), with minor modifications. After X-ray exposure (10min) cells were detached, and 10^4 cells were plated on lethally irradiated feeder layer of 3T3/J2 cells. After 8 days, colonies were fixed, stained with Rhodamine-B (Sigma-Aldrich), and scored under a dissecting microscope. Total colonies were calculated as a percentage of total plated cells (number of colonies x 100/number of cells plated).

Western Blotting and Protein Analysis

MPKs or epidermal tissues (P3), separated from dermis by thermal shock at 65°C for 1min, were lysed in boiling 2%SDS, 50mM Tris/HCl (pH7.4) lysis buffer supplemented with 1mM PMSF, 1mM Na3VO4, 10mM NaF (40). Epidermial tissues were pulverized in liquid nitrogen prior to lysis. Protein concentration was measured using the Bradford assay (Bio-Rad, Hercules, CA, USA). Samples were fractionated on SDS/PAGE and transferred on to PVDF membrane (Merk Millipore, Billerica, MA, USA). Membranes were blocked in 5% non-fat dry milk (Santa Cruz Biotechnology) in Tris-buffer saline, 0.1% Tween20 and incubated with the indicated antibodies following the manufacturer’s instructions.

For immunoblotting the following antibodies were used: rictor, raptor, pSer473Akt, pThr308Akt, panAkt, p-GSK3 α/β (Ser 21/9), p-FOXO 1/3 (Thr32/Thr24), pFoxO1 (Ser256, cross-reactive with Ser193 of FoxO4), pFoxO3 (Ser253),FoxO1, FoxO3, p-TSC2 (Thr1462), total TSC2, mTOR, p-p70S6K (Thr389), total p70S6K, p-4EBP1, total 4EBP1, pPRAS40 (Thr246), p-Erk1/2 (Thr37/46), total Erk1/2, Cleaved Caspase 3, pChk1 (Ser317), total Chk1, pChk2 (Thr68), total Chk2 (Cell Signaling Technology, Danvers, MA, USA); PKCα, Hsp90, p16, p19, p-Ser19 p53, p53 (Santa Cruz Biotechnology); SOD1, SOD2, catalase (Abcam, Cambridge, UK) GAPDH (Merck-Millipore); Vinculin, Tubulin (Sigma-Aldrich); K5 (Covance, Princeton, NJ, USA) and horseradish peroxidase-conjugated secondary antibodies (Sigma-Aldrich). Immunoblots were developed by chemiluminescence with ECL (GE Healthcare, Dharmacon, Lafayette, CO, USA), acquired with the molecular imager ChemiDoc XRS, and quantified by densitometric analysis using the Image-lab software (Bio-Rad). All comparative images of immunoblots were obtained by exposure of the same membranes. Original immunoblots (Figs. S6, S7).

Treatments *in vivo*

For the acute response to 12-*O*-tetradecanoylphorbol-13-acetate (TPA), dorsal skin of 7 weeks old mice of both genotypes were shaved and treated with a single dose of TPA (0.1mM, Sigma-Aldrich) or acetone vehicle alone (56). Treated mice were sacrificed after 48h for histopathological analysis.

For BrdU incorporation analysis in response to TPA, mice were i.p. injected with 50mg/kg of BrdU in sterile PBS, 1h before termination of experiments.

Mice (P3) were X-ray irradiated (full body) with 4 or 8Gy doses and sacrificed for skin analysis 24h later.

For NAC treatment, CT and E-RiKO mice (P2) were i.p. injected with NAC (Sigma) in PBS sterile solution (100mg/kg) or PBS alone daily for 3 days and then irradiated full body (8Gy). Mice were sacrificed and skins were excised 24h after X-ray exposure.

Immunofluorescence and Immunohistochemistry

Skins were fixed in 4% buffered formalin for 24h and embedded in paraffin. 7μm thick skin sections were analyzed as follows: Haematoxylin and Eosin (H&E) staining; IHC was performed for BrdU (DAKO, Carpinteria, CA, USA) and PCNA (Santa Cruz Biotechnology); IF was performed for p63 (Santa Cruz Biotechnology), Loricrin (Covance), TUNEL (Roche, Basel, Switzerland) following manufacturer's instructions. IF samples were counterstained with Dapi or LaminA (Santa Cruz Biotechnology) and mounted in Prolongue reagent (Life Technologies, Carlsbad, CA, USA).

Flow Cytometry

Dead and viable cells were estimated based on AnnexinV/DAPI staining followed by flow cytometry. For this purpose, both adherent and spontaneously detached keratinocytes in each condition were incubated with AnnV-FITC (BD Biosciences) for 30 min in the dark at room temperature and DAPI (Sigma) was added right before the measurement (1μg/ml). Cells were distinguished in live (double negative) and dead: early apoptotic (AnnV+Dapi-), medium/late apoptotic (AnnV+Dapi+) or necrotic (AnnV-DAPI+). Flow cytometric data were acquired using a FACSVerse (Becton Dickinson) and processed with FACSuite software. At least 20,000 events were analyzed for each sample.

Dead cells were calculated by setting to 100% the mean of treated (starvation, epirubicin, X-ray, Cisplatin, Nac/Epirubicin, BPTES/Epirubicin) CT dead cells, obtained by subtracting untreated CT dead cells. The variation of dead cell fraction for each stressor was calculated taking the ratio of treated E-RiKO dead cells (corrected by subtracting untreated

493 E-RiKO dead cells) to treated CT dead cells. Data are representative of at least three
494 independent experiments.
495
496 **Senescence-associated β-galactosidase assay**
497 MPKs were plated in triplicate, cultured for 25 days and stained for β-galactosidase activity
498 using the Senescence Detection Kit (Cell Signaling and Technology) following
499 manufacturer's instructions.
500
501 **X-ray irradiation**
502 Irradiation was done using a Gilardoni RADGIL irradiator (Stationary anode X-ray tube,
503 200kV) at 0.65 Gy/min. MPKs were irradiated at subconfluency in LCM.
504
505 **RNA-Seq**
506 Total RNA was extracted using TRIZOL reagent (Invitrogen) and checked for its integrity
507 by using the DNF-471 Standard Sensitivity RNA Analysis Kit on Fragment Analyzer
508 instrument (Advanced Analytical Technology, Ankeny, IA, USA). RNA-seq libraries were
509 prepared from total RNA using TruSeq RNA Sample Preparation v2 (Illumina, San Diego,
510 CA, USA) according to the manufacturer's protocol and were sequenced on Illumina
511 NextSeq 500 platform (Illumina). Sequencing reads were trimmed out of the low-quality
512 bases with Fastx Toolkit and were mapped on hg19 genome assembly by using TopHat
513 v2.0.6 (Johns-Hopkins University, Baltimore, MD, USA) and mRNAs quantification were
514 performed using Cuffdiff v2.0.2 (University of Maryland, College Park, MD, USA). For
515 further analysis, genes with RPKM<1 in all the samples were filtered out. Gene Ontology
516 was analyzed by using GO web software.
517
518 **Biochemical Analysis of Cell Metabolism:**

519 **Mitochondria extraction** To isolate mitochondrial fractions, cells or pulverized skins were
520 washed twice in ice-cold PBS, lysed in 0.5mL mitochondria lysis buffer (50mmol/L Tris,
521 100mmol/L KCl, 5 mmol/L $MgCl_2$, 1.8 mmol/L ATP, 1 mmol/L EDTA, pH7.2),
522 supplemented with protease inhibitor cocktail III (Calbiochem, La Jolla, CA, USA), 1
523 mmol/L PMSF and 250 mmol/L NaF. Samples were clarified by centrifuging at 650g for
524 3min at +4°C: the supernatant was collected and centrifuged at 13 000g for 5min at +4°C;
525 the pellet – containing mitochondria – was washed once with lysis buffer and resuspended
526 in 0.25mL mitochondria resuspension buffer (250 mmol/L sucrose, 15 mmol/L K_2HPO_4, 2
527 mmol/L $MgCl_2$, 0.5 mmol/L EDTA). A 50 μL aliquot was sonicated and used for the
528 measurement of protein content or Western blotting. To confirm the presence of
529 mitochondrial proteins in the extracts, 10 μg of each sonicated sample were subjected to
530 SDS-PAGE and probed with an anti-porin antibody (Abcam, Cambridge, UK; data not
531 shown).
532 **ROS measurement** ROS amount in whole cells or in mitochondria extracts was measured
533 by labeling samples with the ROS-sensitive fluorescent probe 5-(and-6)-chloromethyl-2',7'-
534 dichlorodihydro-fluorescein diacetate-acetoxymethyl ester (DCFDA-AM). The results were
535 expressed as nmol/mg cell or mitochondrial proteins.
536 **Aldose reductase and NADPH oxidase activity** The activities of aldose reductase and
537 NADPH oxidase were measured by a spectrophotometric assay and by a
538 chemiluminscence-based assay, respectively (57). Results were expressed as nmoles
539 $NADP^+$/min/mg cell proteins for aldose reductase, relative luminescence unit (RLU)/mg cell
540 proteins for NADPH oxidase.
541 **Mitochondrial respiratory chain** To measure the electron flux from complex I to complex
542 III, taken as index of the mitochondrial respiratory activity, 50μg of non-sonicated
543 mitochondrial samples, isolated as previously reported, were re-suspended in 0.2 mL
544 buffer A (5 mmol/L KH_2PO_4, 5 mmol/L $MgCl_2$, 5% w/v bovine serum albumin) and

545 transferred into a quartz spectrophotometer cuvette. Then 0.1 mL buffer B (25% w/v
546 saponin, 50 mmol/L KH_2PO_4, 5 mmol/L $MgCl_2$, 5% w/v bovine serum albumin, 0.12 mmol/L
547 cytochrome c-oxidized form, 0.2 mmol/L NaN_3) was added for 5 min at room temperature.
548 The reaction was started with 0.15 mmol/L NADH and was followed for 5min, reading the
549 absorbance at 550nm by a Packard microplate reader EL340 (Bio-Tek Instruments,
550 Winooski, VT, USA). Results were expressed as nmoles cytochrome c reduced/min/mg
551 mitochondrial protein

552 **ATP levels measurement** The amount of ATP in mitochondrial extracts was measured
553 with the ATP Bioluminescent Assay Kit (Sigma-Aldrich). Results were expressed as
554 nmoles/mg mitochondrial proteins.

555 **Triglycerides levels** The triglyceride amount was measured using the Triglyceride
556 Quantification Kit (Abcam), following the manufacturer's instruction. Results were
557 expressed in nmol/mg cell or tissue proteins, according to the calibration curve previously
558 set.

559 **Fatty acid β-oxidation** The rate of fatty acid β-oxidation was measured by radiolabeling
560 cells or pulverized skins with 2 μ Ci [1-^{14}C]palmitic acid (3.3 mCi/mmol; PerkinElmer,
561 Waltham, MA) and quantifying the amount of ^{14}C-acid soluble metabolites (ASM) by liquid
562 scintillation (57). Results were expressed as pmoles ^{14}C-ASM/h/mg cell proteins.

563 **Glucose uptake and glycolytic metabolism** The uptake of glucose was measured as
564 described earlier (58) and expressed as pmoles 2-deoxy-D-[^{3}H]-glucose/mg cell proteins.
565 HK activity was measured by using the Hexokinase Colorimetric Assay Kit (Sigma-Aldrich).
566 Results were expressed as nmoles NADH/min/mg cell proteins. PFK1 assay was
567 performed according to (59). Results were expressed as nmol NAD^+/min/mg cell proteins.

568 **Glutamine catabolism.** Glutamine catabolism was measured as reported (57). Cells or
569 pulverized skins were washed with PBS, detached by gentle scraping, centrifuged at
570 13,000 x g for 5 min at 4°C, re-suspended in 250 μL of buffer A (150 mmol/L KH_2PO_4, 63

mmol/L Tris/HCl, 0.25 mmol/L EDTA; pH 8.6) and sonicated. The intracellular protein content was measured using the BCA kit (Sigma Chemical Co.). A volume of 100 µL of the whole cell lysates was incubated for 30 min at 37°C in a quartz cuvette, in the presence of 50 µL of 20 mmol/L L-glutamine and 850 µL of buffer B (80 mmol/L Tris/HCl, 20 mmol/L NAD^+, 20 mmol/L ADP, 3% v/v H_2O_2; pH 9.4). The absorbance of NADH was monitored at 340 nm using a Lambda 3 spectrophotometer (PerkinElmer). The kinetics was linear throughout the assay. The results were expressed as µmol NADH/min/mg cell proteins, and were considered as an index of the activity of glutaminase plus L-glutamic dehydrogenase. In a second series of samples, 20 µL of the glutaminase inhibitor bis-2-(5-phenylacetamido-1,3,4-thiadiazol-2-yl)ethyl sulfide BTPES (30 µmol/L) was added after 15 min. This concentration was chosen as it produced 100% inhibition of glutaminase activity in our system (not shown). The absorbance of NADH was monitored for 15 min as described previously. The results, considered as an index of the activity of L-glutamic dehydrogenase, were expressed as µmol NADH/min/mg cell proteins. Glutaminase activity was obtained by subtracting the rate of the second assay from the rate of the first one.

Tricarboxylic acid (TCA) cycle Cells were washed with PBS, detached with trypsin/EDTA (0.05/0.02% v/v) and resuspended in 1 mL Hepes buffer (145 mmol/L NaCl, 5 mmol/L KCl, 1 mmol/L $MgSO_4$, 10 mmol/L Hepes, 10 mmol/L glucose, 1 mmol/L $CaCl_2$, pH 7.4) containing 2 µCi of L-[^{14}C]-glutamine (PerkinElmer) or L-[^{14}C]-glutamate (PerkinElmer). Cell suspensions were incubated for 1 h in a closed experimental system to trap the $^{14}CO_2$ developed from L-[^{14}C]-glutamine or L-[^{14}C]-glutamate and the reaction was stopped by injecting 0.5 mL 0.8 N $HClO_4$. The results were expressed as nmol CO_2/h/mg cell proteins. When indicated, 30 µmol/L of the glutaminase inhibitor BPTES were added to the cell suspension, in order to achieve a 100% inhibition of glutaminase activity.

Glutamine consumption

596 Cells were labelled with 1 µCi [^{14}C]-L-glutamine (PerkinElmer, Waltham, MA) for 30 min,
597 washed five times with ice-cold PBS, detached with trypsin/EDTA, rinsed with 0.5 mL ice-
598 cold PBS and sonicated. A 50 µL aliquot was used to quantify intracellular proteins. [^{14}C]-
599 L-glutamate and [^{14}C]-L-glutamine present within cell lysates were separated by ion
600 exchange chromatography in a 2 mL column. The radioactivity of the eluate containing
601 [^{14}C]-L-glutamate and [^{14}C]-L-glutamine was counted by liquid scintillation and expressed
602 as µmol/mg cellular proteins. The ratio between [^{14}C]-L-glutamate/[^{14}C]-L-glutamine was
603 considered an index of glutamine consumption.
604
605 **Real-time PCR**
606 Total RNA was extracted from epidermis of mice (P3) using Triazol reagent (Invitrogen)
607 according to manufacturer's instructions. Total RNA was reverse-transcribed with a high
608 capacity cDNA reverse transcription kit (Applied BioSystems, Foster city, CA, USA)
609 according to manufacturer's instruction and amplified with specific primers. Taqman PCR
610 reactions were performed using the Universal Probe Library system (Roche Italia, Monza,
611 Italy) on an ABI 7900HT Fast Real Time PCR System (Applied Biosystems). The 18S
612 rRNA pre-developed TaqMan assay (Applied Biosystems) was used as an internal control.
613 Specific primers and UPL probes used are listed in Supplementary informations.
614
615 **Microscopy and Image Analysis**
616 Immunofluorescence analysis was performed on Leica TSCII SP5 confocal microscope
617 (Leica, Wetzlar, Germany) controlled by LAS-AF Software (Leica). Multitrack analysis was
618 used for image acquisition. Histological sections were imaged on Olympus BH-2 RFCA
619 microscope equipped with Leica DFC320 camera (Leica). Camera was controlled by Leica
620 Application Suite version 2.8.1 software (Leica). Phase contrast imaging was performed on
621 Zeiss Axio Observer microscope (Carl Zeiss, Oberkochen, Germany). Quantitative

analysis was performed using ImageJ software (National Institute of Health, Bethesda, MD, USA).

Statistical analysis

Data obtained from densitometric analysis of immunoblots, FACS, IF, CFE and IHC were plotted as mean ± SD. Results were assessed for statistical significance by a standard two-tailed Student's t test as indicated. p values *p< 0.05, **p< 0.005, ***p< 0.0005. For epidermal thickness, measurements obtained from H&E were analyzed with linear regression using Generalized Estimating Equations (GEE) (60) to take into account the correlation between measurements obtained from the same animal. Data obtained from growth assays were analyzed by using the CompareGrowthCurves function included in the R package "statmod": https://cran.r-project.org/web/packages/statmod/index.html

ACKNOWLEDGMENTS

We apologise to the many colleagues whose primary work could not be cited directly due to space constraints. We are thankful to Dr. J. Huelsken for making available K14-Cre transgenic mice. We especially thank P. P. Pandolfi for constant feedback and fruitful discussions and Mara Brancaccio, Valeria Poli, Emilio Hirsch, Alessandra Ghigo for critical reading of the manuscript. This work was supported by Telethon Foundation, Italy (TCP 06001 to E.C.) and by the Italian Association for Cancer Research (AIRC; grant IG 15232 to C.R.). We especially thank Prof. F. Altruda for precious suggestions and support (Prometeo grant ALTF_RIC_ACT_15_01).

CONFLICT OF INTEREST

The authors declare no conflict of interest.

Supplementary information is available at Cell Death and Differentiation's website.

REFERENCES

1. Blanpain C, Fuchs E. Epidermal homeostasis: a balancing act of stem cells in the skin. Nat Rev Mol Cell Biol. 2009 Mar;10(3):207-17.

2. Brandhorst S, Choi IY, Wei M, Cheng CW, Sedrakyan S, Navarrete G, et al. A Periodic Diet that Mimics Fasting Promotes Multi-System Regeneration, Enhanced Cognitive Performance, and Healthspan. Cell Metab. 2015 Jul 7;22(1):86-99.

3. Ristow M, Schmeisser K. Mitohormesis: Promoting Health and Lifespan by Increased Levels of Reactive Oxygen Species (ROS). Dose Response. 2014 May;12(2):288-341.

4. Schulz TJ, Zarse K, Voigt A, Urban N, Birringer M, Ristow M. Glucose restriction extends Caenorhabditis elegans life span by inducing mitochondrial respiration and increasing oxidative stress. Cell Metab. 2007 Oct;6(4):280-93.

5. Zarse K, Schmeisser S, Groth M, Priebe S, Beuster G, Kuhlow D, et al. Impaired insulin/IGF1 signaling extends life span by promoting mitochondrial L-proline catabolism to induce a transient ROS signal. Cell Metab. 2012 Apr 4;15(4):451-65.

6. Sena LA, Chandel NS. Physiological roles of mitochondrial reactive oxygen species. Mol Cell. 2012 Oct 26;48(2):158-67.

7. Strozyk E, Kulms D. The role of AKT/mTOR pathway in stress response to UV-irradiation: implication in skin carcinogenesis by regulation of apoptosis, autophagy and senescence. Int J Mol Sci. 2013;14(8):15260-85.

8. Soeur J, Eilstein J, Lereaux G, Jones C, Marrot L. Skin resistance to oxidative stress induced by resveratrol: from Nrf2 activation to GSH biosynthesis. Free Radic Biol Med. 2015 Jan;78:213-23.

9. Angel P, Szabowski A, Schorpp-Kistner M. Function and regulation of AP-1 subunits in skin physiology and pathology. Oncogene. 2001 Apr 30;20(19):2413-23.

675 10. Zoncu R, Efeyan A, Sabatini DM. mTOR: from growth signal integration to cancer,
676 diabetes and ageing. Nat Rev Mol Cell Biol. 2011 Jan;12(1):21-35.
677 11. Pan Y, Schroeder EA, Ocampo A, Barrientos A, Shadel GS. Regulation of yeast
678 chronological life span by TORC1 via adaptive mitochondrial ROS signaling. Cell Metab.
679 2011 Jun 8;13(6):668-78.
680 12. Wullschleger S, Loewith R, Hall MN. TOR signaling in growth and metabolism. Cell.
681 2006 Feb 10;124(3):471-84.
682 13. Guertin DA, Stevens DM, Thoreen CC, Burds AA, Kalaany NY, Moffat J, et al.
683 Ablation in mice of the mTORC components raptor, rictor, or mLST8 reveals that mTORC2
684 is required for signaling to Akt-FOXO and PKCalpha, but not S6K1. Dev Cell. 2006
685 Dec;11(6):859-71.
686 14. Dann SG, Selvaraj A, Thomas G. mTOR Complex1-S6K1 signaling: at the
687 crossroads of obesity, diabetes and cancer. Trends Mol Med. 2007 Jun;13(6):252-9.
688 15. Sarbassov DD, Guertin DA, Ali SM, Sabatini DM. Phosphorylation and regulation of
689 Akt/PKB by the rictor-mTOR complex. Science. 2005 Feb 18;307(5712):1098-101.
690 16. Jacinto E, Loewith R, Schmidt A, Lin S, Ruegg MA, Hall A, et al. Mammalian TOR
691 complex 2 controls the actin cytoskeleton and is rapamycin insensitive. Nat Cell Biol. 2004
692 Nov;6(11):1122-8.
693 17. Shiota C, Woo JT, Lindner J, Shelton KD, Magnuson MA. Multiallelic disruption of
694 the rictor gene in mice reveals that mTOR complex 2 is essential for fetal growth and
695 viability. Dev Cell. 2006 Oct;11(4):583-9.
696 18. Wang S, Amato KR, Song W, Youngblood V, Lee K, Boothby M, et al. Regulation of
697 endothelial cell proliferation and vascular assembly through distinct mTORC2 signaling
698 pathways. Mol Cell Biol. 2015 Apr;35(7):1299-313.

19. Thomanetz V, Angliker N, Cloetta D, Lustenberger RM, Schweighauser M, Oliveri F, et al. Ablation of the mTORC2 component rictor in brain or Purkinje cells affects size and neuron morphology. J Cell Biol. 2013 Apr 15;201(2):293-308.
20. Kumar A, Harris TE, Keller SR, Choi KM, Magnuson MA, Lawrence JC, Jr. Muscle-specific deletion of rictor impairs insulin-stimulated glucose transport and enhances Basal glycogen synthase activity. Mol Cell Biol. 2008 Jan;28(1):61-70.
21. Yuan M, Pino E, Wu L, Kacergis M, Soukas AA. Identification of Akt-independent regulation of hepatic lipogenesis by mammalian target of rapamycin (mTOR) complex 2. J Biol Chem. 2012 Aug 24;287(35):29579-88.
22. Kumar A, Lawrence JC, Jr., Jung DY, Ko HJ, Keller SR, Kim JK, et al. Fat cell-specific ablation of rictor in mice impairs insulin-regulated fat cell and whole-body glucose and lipid metabolism. Diabetes. 2010 Jun;59(6):1397-406.
23. Huelsken J, Vogel R, Erdmann B, Cotsarelis G, Birchmeier W. beta-Catenin controls hair follicle morphogenesis and stem cell differentiation in the skin. Cell. 2001 May 18;105(4):533-45.
24. Brown J, Wang H, Suttles J, Graves DT, Martin M. Mammalian target of rapamycin complex 2 (mTORC2) negatively regulates Toll-like receptor 4-mediated inflammatory response via FoxO1. J Biol Chem. 2011 Dec 30;286(52):44295-305.
25. Li J, Foitzik K, Calautti E, Baden H, Doetschman T, Dotto GP. TGF-beta3, but not TGF-beta1, protects keratinocytes against 12-O-tetradecanoylphorbol-13-acetate-induced cell death in vitro and in vivo. J Biol Chem. 1999 Feb 12;274(7):4213-9.
26. Orecchia V, Regis G, Tassone B, Valenti C, Avalle L, Saoncella S, et al. Constitutive STAT3 activation in epidermal keratinocytes enhances cell clonogenicity and favours spontaneous immortalization by opposing differentiation and senescence checkpoints. Exp Dermatol. 2015 Jan;24(1):29-34.

724 27. Simunek T, Sterba M, Popelova O, Adamcova M, Hrdina R, Gersl V. Anthracycline-
725 induced cardiotoxicity: overview of studies examining the roles of oxidative stress and free
726 cellular iron. Pharmacol Rep. 2009 Jan-Feb;61(1):154-71.
727 28. Petit-Frere C, Capulas E, Lyon DA, Norbury CJ, Lowe JE, Clingen PH, et al.
728 Apoptosis and cytokine release induced by ionizing or ultraviolet B radiation in primary and
729 immortalized human keratinocytes. Carcinogenesis. 2000 Jun;21(6):1087-95.
730 29. Sotiropoulou PA, Candi A, Mascre G, De Clercq S, Youssef KK, Lapouge G, et al.
731 Bcl-2 and accelerated DNA repair mediates resistance of hair follicle bulge stem cells to
732 DNA-damage-induced cell death. Nat Cell Biol. 2010 Jun;12(6):572-82.
733 30. Song S, Lambert PF. Different responses of epidermal and hair follicular cells to
734 radiation correlate with distinct patterns of p53 and p21 induction. Am J Pathol. 1999
735 Oct;155(4):1121-7.
736 31. Siddik ZH. Cisplatin: mode of cytotoxic action and molecular basis of resistance.
737 Oncogene. 2003 Oct 20;22(47):7265-79.
738 32. Jiang F, Zhang Y, Dusting GJ. NADPH oxidase-mediated redox signaling: roles in
739 cellular stress response, stress tolerance, and tissue repair. Pharmacol Rev. 2011
740 Mar;63(1):218-42.
741 33. Son J, Lyssiotis CA, Ying H, Wang X, Hua S, Ligorio M, et al. Glutamine supports
742 pancreatic cancer growth through a KRAS-regulated metabolic pathway. Nature. 2013 Apr
743 4;496(7443):101-5.
744 34. Yamada T, Egashira N, Bando A, Nishime Y, Tonogai Y, Imuta M, et al. Activation
745 of p38 MAPK by oxidative stress underlying epirubicin-induced vascular endothelial cell
746 injury. Free Radic Biol Med. 2012 Apr 15;52(8):1285-93.
747 35. Allen VW, O'Connor RM, Ulgherait M, Zhou CG, Stone EF, Hill VM, et al. period-
748 Regulated Feeding Behavior and TOR Signaling Modulate Survival of Infection. Curr Biol.
749 2016 Jan 25;26(2):184-94.

750 36. Albert V, Svensson K, Shimobayashi M, Colombi M, Munoz S, Jimenez V, et al.
751 mTORC2 sustains thermogenesis via Akt-induced glucose uptake and glycolysis in brown
752 adipose tissue. EMBO Mol Med. 2016;8(3):232-46.
753 37. Moloughney JG, Kim PK, Vega-Cotto NM, Wu CC, Zhang S, Adlam M, et al.
754 mTORC2 Responds to Glutamine Catabolite Levels to Modulate the Hexosamine
755 Biosynthesis Enzyme GFAT1. Mol Cell. 2016 Sep 1;63(5):811-26.
756 38. van der Vos KE, Eliasson P, Proikas-Cezanne T, Vervoort SJ, van Boxtel R, Putker
757 M, et al. Modulation of glutamine metabolism by the PI(3)K-PKB-FOXO network regulates
758 autophagy. Nat Cell Biol. 2012 Aug;14(8):829-37.
759 39. Tran H, Brunet A, Grenier JM, Datta SR, Fornace AJ, Jr., DiStefano PS, et al. DNA
760 repair pathway stimulated by the forkhead transcription factor FOXO3a through the
761 Gadd45 protein. Science. 2002 Apr 19;296(5567):530-4.
762 40. Iglesias-Bartolome R, Patel V, Cotrim A, Leelahavanichkul K, Molinolo AA, Mitchell
763 JB, et al. mTOR inhibition prevents epithelial stem cell senescence and protects from
764 radiation-induced mucositis. Cell Stem Cell. 2012 Sep 7;11(3):401-14.
765 41. Belikova NA, Glumac A, Rafikov R, Jiang J, Greenberger JS, Kagan VE, et al.
766 Radioprotection by short-term oxidative preconditioning: role of manganese superoxide
767 dismutase. FEBS Lett. 2009 Nov 3;583(21):3437-42.
768 42. Berge U, Kristensen P, Rattan SI. Hormetic modulation of differentiation of normal
769 human epidermal keratinocytes undergoing replicative senescence in vitro. Exp Gerontol.
770 2008 Jul;43(7):658-62.
771 43. Gu Y, Lindner J, Kumar A, Yuan W, Magnuson MA. Rictor/mTORC2 is essential for
772 maintaining a balance between beta-cell proliferation and cell size. Diabetes. 2011
773 Mar;60(3):827-37.

774 44. Carr TD, Feehan RP, Hall MN, Ruegg MA, Shantz LM. Conditional disruption of
775 rictor demonstrates a direct requirement for mTORC2 in skin tumor development and
776 continued growth of established tumors. Carcinogenesis. 2015 Apr;36(4):487-97.
777 45. Zelenka J, Dvorak A, Alan L. L-Lactate Protects Skin Fibroblasts against Aging-
778 Associated Mitochondrial Dysfunction via Mitohormesis. Oxid Med Cell Longev.
779 2015;2015:351698.
780 46. Harrison DE, Strong R, Sharp ZD, Nelson JF, Astle CM, Flurkey K, et al.
781 Rapamycin fed late in life extends lifespan in genetically heterogeneous mice. Nature.
782 2009 Jul 16;460(7253):392-5.
783 47. Robida-Stubbs S, Glover-Cutter K, Lamming DW, Mizunuma M, Narasimhan SD,
784 Neumann-Haefelin E, et al. TOR signaling and rapamycin influence longevity by regulating
785 SKN-1/Nrf and DAF-16/FoxO. Cell Metab. 2012 May 2;15(5):713-24.
786 48. Sarbassov DD, Ali SM, Sengupta S, Sheen JH, Hsu PP, Bagley AF, et al.
787 Prolonged rapamycin treatment inhibits mTORC2 assembly and Akt/PKB. Mol Cell. 2006
788 Apr 21;22(2):159-68.
789 49. Niles BJ, Joslin AC, Fresques T, Powers T. TOR complex 2-Ypk1 signaling
790 maintains sphingolipid homeostasis by sensing and regulating ROS accumulation. Cell
791 Rep. 2014 Feb 13;6(3):541-52.
792 50. Soukas AA, Kane EA, Carr CE, Melo JA, Ruvkun G. Rictor/TORC2 regulates fat
793 metabolism, feeding, growth, and life span in Caenorhabditis elegans. Genes Dev. 2009
794 Feb 15;23(4):496-511.
795 51. Carr TD, DiGiovanni J, Lynch CJ, Shantz LM. Inhibition of mTOR suppresses UVB-
796 induced keratinocyte proliferation and survival. Cancer Prev Res (Phila). 2012
797 Dec;5(12):1394-404.

52. D'Errico M, Teson M, Calcagnile A, Nardo T, De Luca N, Lazzari C, et al. Differential role of transcription-coupled repair in UVB-induced response of human fibroblasts and keratinocytes. Cancer Res. 2005 Jan 15;65(2):432-8.
53. Selvarajah J, Nathawat K, Moumen A, Ashcroft M, Carroll VA. Chemotherapy-mediated p53-dependent DNA damage response in clear cell renal cell carcinoma: role of the mTORC1/2 and hypoxia-inducible factor pathways. Cell Death Dis. 2013 Oct 17;4:e865.
54. Lee JS, Vo TT, Fruman DA. Targeting mTOR for the treatment of B cell malignancies. Br J Clin Pharmacol. 2016 Jan 25.
55. Saoncella S, Tassone B, Deklic E, Avolio F, Jon C, Tornillo G, et al. Nuclear Akt2 opposes limbal keratinocyte stem cell self-renewal by repressing a FOXO-mTORC1 signaling pathway. Stem Cells. 2014 Mar;32(3):754-69.
56. Li J, Wei Y, Wagner TE. In vitro endothelial differentiation of long-term cultured murine embryonic yolk sac cells induced by matrigel. Stem Cells. 1999;17(2):72-81.
57. Capello M, Ferri-Borgogno S, Riganti C, Chattaragada MS, Principe M, Roux C, et al. Targeting the Warburg effect in cancer cells through ENO1 knockdown rescues oxidative phosphorylation and induces growth arrest. Oncotarget. 2015 Dec 30.
58. Bergandi L, Silvagno F, Russo I, Riganti C, Anfossi G, Aldieri E, et al. Insulin stimulates glucose transport via nitric oxide/cyclic GMP pathway in human vascular smooth muscle cells. Arterioscler Thromb Vasc Biol. 2003 Dec;23(12):2215-21.
59. Sharma B. Kinetic Characterisation of Phosphofructokinase Purified from Setaria cervi: A Bovine Filarial Parasite. Enzyme Res. 2011;2011:939472.
60. Hanley JA, Negassa A, Edwardes MD, Forrester JE. Statistical analysis of correlated data using generalized estimating equations: an orientation. Am J Epidemiol. 2003 Feb 15;157(4):364-75.

824

825

825

826 **Figure Legends**

827

828 Figure 1

829 **Loss of rictor/mTORC2 in the epidermis results in tissue hypoplasia and impaired**

830 **TPA response.**

831 a) Diagram of the breeding strategy used to obtain K-14 cre mediated homozygous

832 deletion of rictor (E-RiKO). WT: wild-type mouse, CT: WT mouse with exon 3 flanked by

833 two LoxP sites. White tile: hexon; Black arrowhead: LoxP site. b-c) Representative

834 Western blotting analysis with the indicated antibodies of: b) Epidermal extracts of CT and

835 E-RiKO newborn (P3) littermates (n=3); c) Cell extracts of CT and E-RiKO MPKs

836 subjected to starvation/stimulation treatment for the indicated times. d-e) Skins of E-RiKO

837 and CT littermates (P3): d) Representative H&E staining (left panels) and histograms of

838 the epidermal thickness. Epi: epidermis. Der: dermis. Bar: 30μm. e) PCNA staining (left

839 panels) and histograms of the percentage of $PCNA^+$ epidermal area. Arrows: brightest

840 $PCNA^+$ cells in epidermal basal layers. Bar: 50μm. f) Representative H&E images of skin

841 section obtained from E-RiKO and CT littermates (7-weeks old) upon 48h of TPA or

842 vehicle treatment, (n=3). Bar: 30μm. Histograms represent epidermal thickness. g)

843 Representative confocal images of IF performed on skin sections, obtained from mice

844 treated as in f) and injected with BrdU for the final hour of the experiment, with anti-BrdU

845 antibody (red) and counterstained with anti-LaminA antibody (green). Arrowheads: $BrdU^+$

846 cells. Bar: 50μm. The percentage of $BrdU^+$ cells/area (μm^2) was quantified (right

847 histograms).

848 Quantification of epidermal thickness (mean ± SEM) for 3 mice/genotype; the standard

849 error and the significance of the differences between groups were determined with linear

850 regression using GEE. ***$p<0.0005$.

PCNA and BrdU histograms represent the mean ± SD of 30 fields/genotype (n=3). ***p<0.0005.

Figure 2

Rictor-deficient keratinocytes display reduced proliferation and delayed senescence *in vitro.*

a) Quantification of MPKs derived from at least 10 skins of CT and E-RiKO newborn mice (P3). Histograms represent mean ± SD. ***p<0.0005. E-RiKO and CT MPKs were isolated from littermates P3 (n=5) and analyzed as follows: b) Growth curve: MPKs (both adherent and suspended/differentiated cells) were detached and counted at the indicated times upon plating. Data are mean ± SD obtained from triplicate samples/genotype of three independent experiments. CompareGrowthCurve function was used (see Materials and Methods). p=0.029. c) Confluent MPKs, were subjected to a single BrdU pulse (3h) under basal conditions. Histograms represent mean ± SD of the percentage of $BrdU^+$ cells determined from at least 200 cells/genotype of three independent experiments. ***p<0.0005. d) Representative phase contrast images of MPKs cultured in LCM for the indicated times. Note that E-RiKO cells show at 3 days reduced density compared to CT counterparts, at 5-10 days they display a comparable confluency, while at 25 days they maintained an undifferentiated proliferative morphology whereas CT cells show a flattened, senescent appearance. Bar: 100μm. e) Western blotting analysis for the indicated markers of MPKs extracts of 25-day cultures. f) Representative images of 25-day old MPKs stained for SA-βGal (left panel). The percentage of SA-βGal^+ cells is quantified in the histograms (right) as mean ± SD of at least 200 cells/genotype of three independent experiments. Bar: 50μm. *p<0.05.

Figure 3

Rictor-deficient keratinocytes display resistance to death-inducing stimuli both *in vitro* and *in vivo.*

a-h) E-RiKO and CT MPKs (P3) were analyzed at confluency (5-6 days in culture) as follows:

a) Representative Western blotting analysis of extracts obtained from E-RiKO and CT MPKs upon starvation (st) for the apoptosis marker cleaved caspase 3 (Cl-casp3) and Rictor. Loading control: Tubulin. b) Representative Annexin-V/DAPI flow cytometry plots of E-RiKO and CT MPKs kept in complete LCM (-) or starvation (St) for 72h. Histograms are mean ± SD of dead cells expressed as variation of the fraction of dead cells in response to starvation (72h) (see Materials and Methods) *p<0.05. c-d) MPKs grown in LCM for 24h were kept untreated (-) or treated with epirubicin (10μM) for 18h: c) Representative Western blotting analysis for the indicated proteins. d) Representative AnnexinV/DAPI flow cytometry plots of E-RiKO and CT MPKs kept untreated (-) or treated with Epirubicin for 15h. Histograms are mean ± SD of dead cells determined as in b). *p<0.05. e) MPKs maintained in LCM or starved (St) for 18h were treated with a single BrdU pulse. $BrdU^+$ cells were determined out of 200 cells ($Dapi^+$)/genotype in three independent experiments. Histograms represent mean ± SD of $BrdU^+$ cells. Note that upon St 18h cells display comparable BrdU uptake. *p<0.05; ***p<0.0005. f) MPKs were starved as in e) and then treated with the indicated doses of epirubicin for 4h. Cell extracts were analysed by western blotting for Rictor, Cl-casp3 and Tubulin, loading control. Ratio between Cl-casp3 and Tubulin is reported. g) Histograms represent mean colony number ± SD from duplicate plates determined in untreated (-) and treated (X-ray) MPKs colony forming efficiency assay, relative to the value obtained with CT (-) cells set as unitary. Data are representative of at least two independent experiments. ***p<0.0005, **p<0.005. h) Representative AnnexinV/DAPI flow cytometry plots of E-RiKO and CT MPKs kept

901 untreated (-) or X-ray treated (60Gy) analysed after 96h. Histograms are mean ± SD of
902 dead cells determined as in b) *p<0.05. i) Representative confocal images for TUNEL (red)
903 and Dapi (blue) stainings of skin sections obtained from E-RiKO and CT littermates (P3)
904 subjected to a full body single dose of X-ray radiation (8Gy) and sacrificed 24h later. Bar:
905 100μm. n=5mice/genotype. j) Quantification of TUNEL staining of X-ray treated skins with
906 and 4Gy and 8Gy as in j). Histograms represent mean ± SD of $TUNEL^+$ cells/area
907 ($10^3 \mu m^2$) of at least 30 hair follicles of 4 mice/genotype. Note that the $TUNEL^+$ area was
908 limited to the hair follicle matrix, with similar cellular density and sensitive to
909 radiations.***p<0.0005.
910
911 Figure 4
912 **RNA-Seq analysis of rictor-deficient keratinocytes suggests a link between**
913 **metabolic changes and stress adaptation.**
914 E-RiKO and CT MPKs were isolated from newborn littermates (n=6/genotype), grown in
915 LCM and analyzed by RNA–Seq analysis under basal conditions (24h LCM) and upon X-
916 ray exposure (8Gy) for 1h and 24h. a) Upregulated and downregulated genes detected in
917 E-RiKO versus CT cells under basal conditions. b) Selected gene ontology (GO)
918 categories enriched in differentially expressed genes as in a). The number of genes
919 belonging to each GO category is indicated. Rictor deficiency was coupled with
920 downregulation of genes involved in lipid metabolism (P=1.08E-16), keratinocyte
921 differentiation (P=1.68E-9), oxidation-reduction process (P=1.89E-6), lipid catabolic
922 process (P=2.41E-6), lipid biosynthetic process (P=2.7E-6) and upregulation of genes
923 involved in cell motility (P=2.62E-18), signal transduction (P=3.15E-15), inflammatory
924 response (P=1.66E-12), response to stress (P=3.11E-7) and defense response (P=2.28E-
925 6) (Fig.4b). c) Upregulated and downregulated genes of X-ray treated MPKs of the
926 indicated genotype relative to basal conditions. d) Differentially regulated genes overlap

927 between CT MPKs X-ray treated for 1h and E-RiKO MPKs under basal conditions (27.5%
928 gene overlap; P=5.44E-57, Fisher exact test). e) Selected GO categories enriched in
929 overlapping differentially regulated genes (DEGs) subgroup as in d).
930
931 Figure 5
932 **Rictor-deficient keratinocytes display metabolic reprogramming.**
933 E-RiKO and CT MPKs, isolated and cultured in LCM (n=5 littermates P3/genotype), were
934 analyzed at confluency upon LCM 24h as follows: a) Total cellular ROS (nmol/mg prot), b)
935 Mitochondrial ROS (nmol/mg mit prot); c) Mitochondrial/Total ROS (%) determined by
936 compairing mitochondrial and total ROS, each normalized for total protein content; d)
937 Aldose reductase (nmol $NADP^+$/min/mg prot); e) NADPH oxidase (RLU/mg prot); f)
938 Electron transport chain (nmol red cit c/min/mg mit prot); g) ATP (nmol/mg mit prot); h)
939 Lipid β-oxidation (pmol/h/mg prot); i) Triglycerides (nmol/mg prot); j) Glucose uptake (pmol
940 glucose/mg prot); k) Hexokinase (nmol NADH/min/mg prot); l) Phosphofructose kinase 1
941 (nmol NAD^+/min/mg prot); m) Glutaminase (μmol NADH/min/mg prot); n) Glutamic
942 dehydrogenase (μmol NADH/min/mg prot); o) TCA cycle with [14C] glutamine (pmol
943 CO_2/h/mg mit prot); p) TCA cycle with [14C] glutamate (pmol CO_2/h/mg mit prot); q)
944 Intracellular [14C]glutamine (μmol/mg prot); r) Intracellular [14C]glutamate (μmol/mg prot);
945 s) Glutamate/glutamate ratio; t) Total SOD (μmol/min/mg prot); u) Catalase (nmol/min/mg
946 prot); v) Mitochondrial SOD (μmol/min/mg prot).
947 All histograms represent mean ± SD of the indicated metabolic parameters determined in
948 at least three independent experiments. ***p<0.0005; **p<0.005; *p<0.05.
949

Figure 6

ROS scavenging and glutaminase inhibition sensitize rictor-deficient keratinocytes to epirubicin-induced cell death.

E-RiKO and CT MPKs were isolated (n=5/genotype), grown in LCM and analyzed at confluency for: a) Total cellular ROS was measured upon LCM (-) or NAC 10mM for 48h. Histograms represent mean ± SD of ROS levels measured in at least three independent experiments. ***p<0.0005; *p<0.05. b) Histograms represent mean ± SD of mitochondrial ROS determined in cells treated as in a). c) Representative Western blotting analysis for the indicated antibodies of cell extracts obtained from MPKs maintained as in a) and subsequently treated with DMSO (-) or epirubicin 10μM for 10h. Ratio between Cl-casp3 and keratin5 (K5) is reported. d) Representative AnnexinV/DAPI flow cytometry plots of E-RiKO and CT MPKs maintained untreated (-) or pre-treated with NAC and subsequently treated with epirubicin 10μM for 15h. Histograms are mean ± SD of dead cells determined as described in Materials and Methods. *p<0.05. e) Histograms represent the mean ± SD of the glutaminase activity (μmol NADH/min/mg prot) evaluated in CT and E-RiKO MPKs treated with BPTES (10μM, 2h) in at least three independent experiments.**p<0.005, *p<0.05. f) Histograms represent mean ± SD of total ROS levels (nmol/mg prot) measured in cells treated as in e) in at least three independent experiments. *p<0.05. g) Representative Western blotting analysis with the indicated antibodies of cell extracts derived from E-RiKO and CT cells pre-treated with BPTES at the indicated doses for 48h and exposed to epirubicin in the presence of BPTES for 15h. Ratio between Cl-casp3 and keratin5 (K5) is reported. h) Representative AnnexinV/DAPI flow cytometry plots of E-RiKO and CT MPKs maintained untreated (-) or pre-treated with BPTES and subsequently

974 treated with epirubicin 10μM for 15h. Histograms are mean ± SD of dead cells as in d).
975 **p<0.005, *p<0,05.
976
977 Figure 7
978 **Rictor-deficient epidermis displays a metabolic rewiring and ROS-dependent lower**
979 **sensitivity to stress.**
980 a)Metabolic analysis of CT and E-RiKO skins obtained from at least 3mice/genotype.
981 Histograms represent mean ± SD of the following metabolic parameters: total cellular ROS
982 (nmol/mg prot); Mitochondrial ROS (nmol/mg mit prot); Electron transport chain (nmol red
983 cit c/min/mg mit prot); ATP (nmol/mg mit prot); Lipid β-oxidation (pmol/h/mg prot);
984 Hexokinase (nmol NADH/min/mg prot); Glutaminase (μmol NADH/min/mg prot); Glutamic
985 dehydrogenase (μmol NADH/min/mg prot). **p<0.005, *p<0.05. b) RNA was extracted
986 from CT and E-RiKO skins of at least 6mice/genotype and RT-PCR analysis for the
987 following genes was performed: Gadd45-α; Gadd45-β; Gadd45-γ; Glul; Il1-α; Acsl1; Faah;
988 Fabp4. Data are represented as mean ± SD of the fold change relative to unitary value
989 assigned to CT. **p<0.005, *p<0.05.
990 c) Representative confocal images of IF for TUNEL (red) and Dapi (blue) stainings on E-
991 RiKO and CT skin sections pre-treated with NAC (or vehicle) for 48h (i.p. injection),
992 subjected to a single dose of X-ray radiation (8Gy) and collected 24h later. Bar: 100μm.
993 n=10mice/genotype. d) Histograms represent mean ±SD of ROS levels (nmol/mg prot) in
994 CT and E-RiKO skins treated with NAC (or vehicle) for 48h, of 3mice/genotype. *p<0.05,
995 **p<0.005. e) Histograms represent mean ± SD of $TUNEL^+$ cells/area ($10^3 \mu m^2$) of at least
996 30 hair follicles of 10 mice/genotype treated as in c). ***p<0.0005.
997
998
999 **Supplementary information is available at Cell Death and Differentiation's website.**

1000

Figure Legends

Figure 1

Loss of rictor/mTORC2 in the epidermis results in tissue hypoplasia and impaired TPA response.

a) Diagram of the breeding strategy used to obtain K-14 cre mediated homozygous deletion of rictor (E-RiKO). WT: wild-type mouse, CT: WT mouse with exon 3 flanked by two LoxP sites. White tile: hexon; Black arrowhead: LoxP site. b-c) Representative Western blotting analysis with the indicated antibodies of: b) Epidermal extracts of CT and E-RiKO littermates (P3, n=3); c) Cell extracts of CT and E-RiKO MPKs subjected to starvation/stimulation treatment for the indicated times. d-e) Skins of E-RiKO and CT littermates (P3): d) Representative H&E staining (left panels) and histograms of the epidermal thickness. Epi: epidermis. Der: dermis. Bar: 30μm. e) PCNA staining (left panels) and histograms of the percentage of $PCNA^+$ epidermal area. Arrows: brightest $PCNA^+$ cells. Bar: 50μm. f) Representative H&E images of skin section obtained from E-RiKO and CT littermates (7-weeks old) upon 48h of TPA or vehicle treatment, (n=3). Bar: 30μm. Histograms represent epidermal thickness. g) Representative confocal images of IF performed on skin sections, obtained from mice treated as in f) and injected with BrdU for the final hour of the experiment, with anti-BrdU antibody (red) and counterstained with anti-LaminA antibody (green). Arrowheads: $BrdU^+$ cells. Bar: 50μm. The percentage of $BrdU^+$ cells/area (μm^2) was quantified (right histograms).

Quantification of epidermal thickness (mean ± SEM) for 3 mice/genotype performed with GEE statistical analysis. ***p<0.0005.

PCNA and BrdU histograms represent the mean ± SD of 30 fields/genotype (n=3). ***p<0.0005.

Figure 2

Rictor-deficient keratinocytes display reduced proliferation and delayed senescence *in vitro.*

a) Quantification of MPKs derived from at least 10 skins of CT and E-RiKO mice (P3). Histograms represent mean ± SD. ***p<0.0005. E-RiKO and CT MPKs were isolated from littermates P3 (n=5) and analyzed as follows: b) Growth curve: MPKs (both adherent and suspended/differentiated cells) were detached and counted at the indicated times upon plating. Data are mean ± SD obtained from triplicate samples/genotype of three independent experiments. CompareGrowthCurve function was used, see Materials and Methods. p=0.029. c) Confluent MPKs, were subjected to a single BrdU pulse (3h) under basal conditions. Histograms represent mean ± SD of the percentage of $BrdU^+$ cells determined from at least 200 cells/genotype of three independent experiments. ***p<0.0005. d) Representative phase contrast images of MPKs cultured in LCM for the indicated times. Note that E-RiKO cells show at 3 days reduced density compared to CT counterparts, at 5-10 days they display a comparable confluency, while at 25 days they maintained an undifferentiated proliferative morphology whereas CT cells show a senescent appearance. Bar: 100μm. e) Western blotting analysis for the indicated markers of MPKs extracts of 25-day cultures. f) Representative images of 25-day old MPKs stained for SA-βGal (left panel). The percentage of SA-βGal^+ cells is quantified in the histograms (right) as mean ± SD of at least 200 cells/genotype of three independent experiments. Bar: 50μm. *p<0.05.

Figure 3

Rictor-deficient keratinocytes display resistance to death-inducing stimuli both *in vitro* and *in vivo.*

a-h) E-RiKO and CT MPKs (P3) were analyzed at confluency (5-6 days in culture) as follows:

a) Representative Western blotting analysis of extracts obtained from E-RiKO and CT MPKs upon starvation (st) for the apoptosis marker cleaved caspase 3 (Cl-casp3) and Rictor. Loading control: Tubulin. b) Representative Annexin-V/DAPI flow cytometry plots of E-RiKO and CT MPKs under basal conditions (-) or 72h starvation (St 72h). Histograms are mean ± SD of dead cells (CT and E-RiKO MPKs) expressed as percentage of variation of dead cells fraction in response to starvation 72h, in three independent experiments. c-d) MPKs grown in LCM for 24h were kept untreated (-) or treated with epirubicin (10μM) for 18h: c) Representative Western blotting analysis for the indicated proteins. d) Representative AnnexinV/DAPI flow cytometry plots of E-RiKO and CT MPKs under basal conditions (-) or Epirubicin for 15h. Histograms are mean ± SD of dead cells (CT and E-RiKO MPKs) expressed as percentage of variation of dead cells fraction in response to Epirubicin, in three independent experiments. e) MPKs maintained in LCM or starved (St) for 18h were treated with a single BrdU pulse. $BrdU^+$ cells were determined out of 200 cells ($Dapi^+$)/genotype in three independent experiments. Histograms represent mean ± SD of $BrdU^+$ cells. Note that upon St 18h cells display comparable BrdU uptake. *$p<0.05$; ***$p<0.0005$. f) MPKs were starved as in e) and then treated with the indicated doses of epirubicin for 4h. Cell extracts were analysed by western blotting for Rictor, Cl-casp3 and Tubulin, loading control. Ratio between Cl-casp3 and Tubulin is reported. g) Histograms represent mean colony number ± SD from duplicate plates determined in untreated (-) and treated (X-ray) MPKs colony forming efficiency assay, relative to the value obtained with CT (-) cells set as unitary. Data are representative of at least two independent experiments. ***$p<0.0005$, **$p<0.005$. h) Representative AnnexinV/DAPI flow cytometry plots of E-RiKO and CT MPKs under basal conditions (-) or X-ray treatment (60Gy). Histograms are mean ± SD of dead cells (CT and E-RiKO MPKs) expressed as percentage of variation of dead

cells fraction in response to X-ray, in three independent experiments. i) Representative confocal images for TUNEL (red) and Dapi (blue) stainings of skin sections obtained from E-RiKO and CT littermates (P3) subjected to a full body single dose of X-ray radiation (8Gy) and sacrificed 24h later. Bar: 100μm. n=5mice/genotype. j) Quantification of TUNEL staining of X-ray treated skins with and 4Gy and 8Gy as in j). Histograms represent mean ± SD of $TUNEL^+$ cells/area ($10^3\mu m^2$) of at least 30 hair follicles of 4 mice/genotype. Note that the $TUNEL^+$ area was limited to the hair follicle matrix, with similar cellular density and sensitive to radiations (46, 47). ***p<0.0005.

Figure 4

RNA-Seq analysis of rictor-deficient keratinocytes suggests a link between metabolic changes and stress adaptation.

E-RiKO and CT MPKs were isolated from newborn littermates (n=6/genotype), grown in LCM and analyzed by RNA–Seq analysis under basal conditions (24h LCM) and upon X-ray exposure (8Gy) for 1h and 24h. a) Upregulated and downregulated genes detected in E-RiKO versus CT cells under basal conditions. b) Selected gene ontology (GO) categories enriched in differentially expressed genes as in a). The number of genes belonging to each GO category is indicated. c) Upregulated and downregulated genes of X-ray treated MPKs of the indicated genotype relative to basal conditions. d) Differentially regulated genes overlap between CT MPKs X-ray treated for 1h and E-RiKO MPKs under basal conditions. e) Selected GO categories enriched in overlapping differentially regulated genes (DEGs) subgroup as in d).

Figure 5

Rictor-deficient keratinocytes display metabolic reprogramming.

E-RiKO and CT MPKs, isolated and cultured in LCM (n=5 littermates P3/genotype), were analyzed at confluency upon LCM 24h as follows: a) Total cellular ROS (nmol/mg prot), b) Mitochondrial ROS (nmol/mg mit prot); c) Mitochondrial/Total ROS (%) determined by compairing mitochondrial and total ROS, each normalized for total protein content; d) Aldose reductase (nmol $NADP^+$/min/mg prot); e) NADPH oxidase (RLU/mg prot); f) Electron transport chain (nmol red cit c/min/mg mit prot); g) ATP (nmol/mg mit prot); h) Lipid β-oxidation (pmol/h/mg prot); i) Triglycerides (nmol/mg prot); j) Glucose uptake (pmol glucose/mg prot); k) Hexokinase (nmol NADH/min/mg prot); l) Phosphofructose kinase 1 (nmol NAD^+/min/mg prot); m) Glutaminase (μmol NADH/min/mg prot); n) Glutamic dehydrogenase (μmol NADH/min/mg prot); o) TCA cycle with [14C] glutamine (pmol CO_2/h/mg mit prot); p) TCA cycle with [14C] glutamate (pmol CO_2/h/mg mit prot); q) Intracellular [14C]glutamine (μmol/mg prot); r) Intracellular [14C]glutamate (μmol/mg prot); s) Glutamate/glutamate ratio; t) Total SOD (μmol/min/mg prot); u) Catalase (nmol/min/mg prot); v) Mitochondrial SOD (μmol/min/mg prot).

All histograms represent mean ± SD of the indicated metabolic parameters determined in at least three independent experiments. ***p<0.0005; **p<0.005; *p<0.05.

Figure 6

ROS scavenging and glutaminase inhibition sensitize rictor-deficient keratinocytes to Epirubicin-induced cell death.

E-RiKO and CT MPKs were isolated (n=5/genotype), grown in LCM and analyzed at confluency for: a) Total cellular ROS was measured upon LCM (-) or NAC 10mM for 48h. Histograms represent mean ± SD of ROS levels measured in at least three independent experiments. ***p<0.0005; *p<0.05. b) Histograms represent mean ± SD of mitochondrial ROS determined in cells treated as in a). c) Representative Western blotting analysis for the indicated antibodies of cell extracts obtained from MPKs maintained as in a) and

subsequently treated with DMSO (-) or epirubicin 10μM for 10h. Ratio between Cl-casp3 and keratin5 (K5) is reported. d) Representative AnnexinV/DAPI flow cytometry plots of E-RiKO and CT MPKs maintained untreated (-) or pre-treated with NAC and subsequently treated with Epirubicin 10μM for 15h. Histograms are mean ± SD of dead cells (CT and E-RiKO MPKs) expressed as percentage of variation of dead cells fraction in response to NAC and Epirubicin, in three independent experiments. e) Histograms represent the mean ± SD of the glutaminase activity (μmol NADH/min/mg prot) evaluated in CT and E-RiKO MPKs treated with BPTES (10μM, 2h) in at least three independent experiments.**p<0.005, *p<0.05. f) Histograms represent mean ± SD of total ROS levels (nmol/mg prot) measured in cells treated as in e) in at least three independent experiments. *p<0.05. g) Representative Western blotting analysis with the indicated antibodies of cell extracts derived from E-RiKO and CT cells pre-treated with BPTES at the indicated doses for 48h and exposed to epirubicin in the presence of BPTES for 15h. Ratio between Cl-casp3 and keratin5 (K5) is reported. h) Representative AnnexinV/DAPI flow cytometry plots of E-RiKO and CT MPKs maintained untreated (-) or pre-treated with BPTES and subsequently treated with Epirubicin 10μM for 15h. Histograms are mean ± SD of dead cells (CT and E-RiKO MPKs) expressed as percentage of variation of dead cells fraction in response to BPTES and Epirubicin, in three independent experiments. **p<0.005, *p<0,05.

Figure 7

Rictor-deficient epidermis displays a metabolic rewiring and ROS-dependent lower sensitivity to stress.

a)Metabolic analysis of CT and E-RiKO skins obtained from at least 3mice/genotype. Histograms represent mean ± SD of the following metabolic parameters: total cellular ROS (nmol/mg prot); Mitochondrial ROS (nmol/mg mit prot); Electron transport chain (nmol red cit c/min/mg mit prot); ATP (nmol/mg mit prot); Lipid β-oxidation (pmol/h/mg prot);

Hexokinase (nmol NADH/min/mg prot); Glutaminase (μmol NADH/min/mg prot); Glutamic dehydrogenase (μmol NADH/min/mg prot). **p<0.005, *p<0.05. b) RNA was extracted from CT and E-RiKO skins of at least 6mice/genotype and RT-PCR analysis for the following genes was performed: Gadd45-a; Gadd45-b; Gadd45-g; Glul; Il1-a; Acsl1; Faah; Fabp4. Data are represented as mean ± SD. **p<0.005, *p<0.05.
c) Representative confocal images of IF for TUNEL (red) and Dapi (blue) stainings on E-RiKO and CT skin sections pre-treated with NAC (or vehicle) for 48h (i.p. injection), subjected to a single dose of X-ray radiation (8Gy) and collected 24h later. Bar: 100μm. n=10mice/genotype. d) Histograms represent mean ±SD of ROS levels (nmol/mg prot) in CT and E-RiKO skins treated with NAC (or vehicle) for 48h, of 3mice/genotype. *p<0.05, **p<0.005. e) Histograms represent mean ± SD of $TUNEL^+$ cells/area ($10^3\mu m^2$) of at least 30 hair follicles of 10 mice/genotype treated as in c). ***p<0.0005.

Supplementary information is available at Cell Death and Differentiation's website.

Figure 1

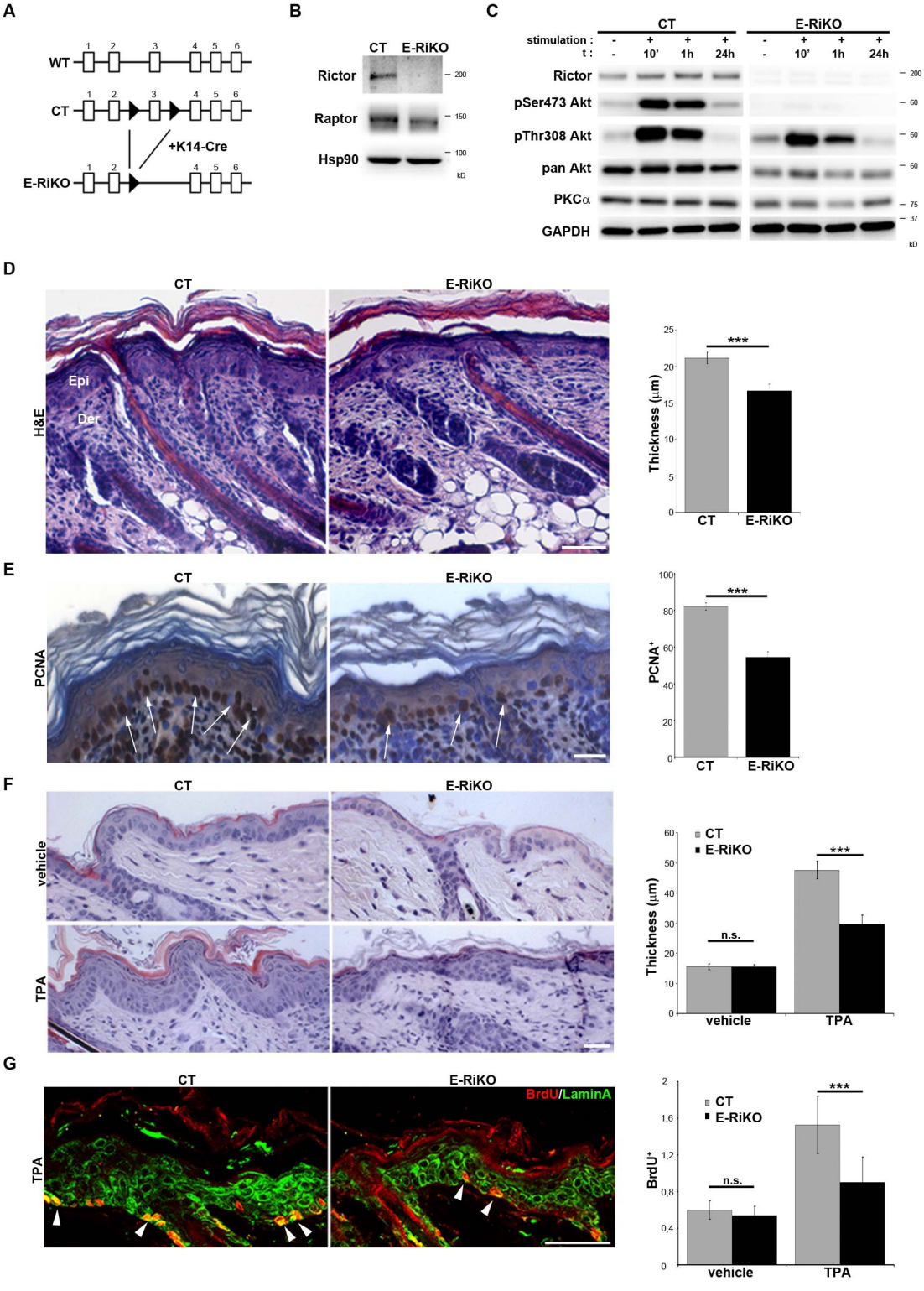
A
WT
CT
+K14-Cre
E-RiKO
B
CT
E-RiKO
Rictor
Raptor
Hsp90
C
CT
E-RiKO
stimulation :
t :
Rictor
pSer473 Akt
pThr308 Akt
pan Akt
PKCα
GAPDH
kD
D
CT
E-RiKO
H&E
Epi
Der
Thickness (μm)
***
E
PCNA
PCNA+
F
vehicle
TPA
n.s.
G
BrdU/LaminA
BrdU+

Figure 2

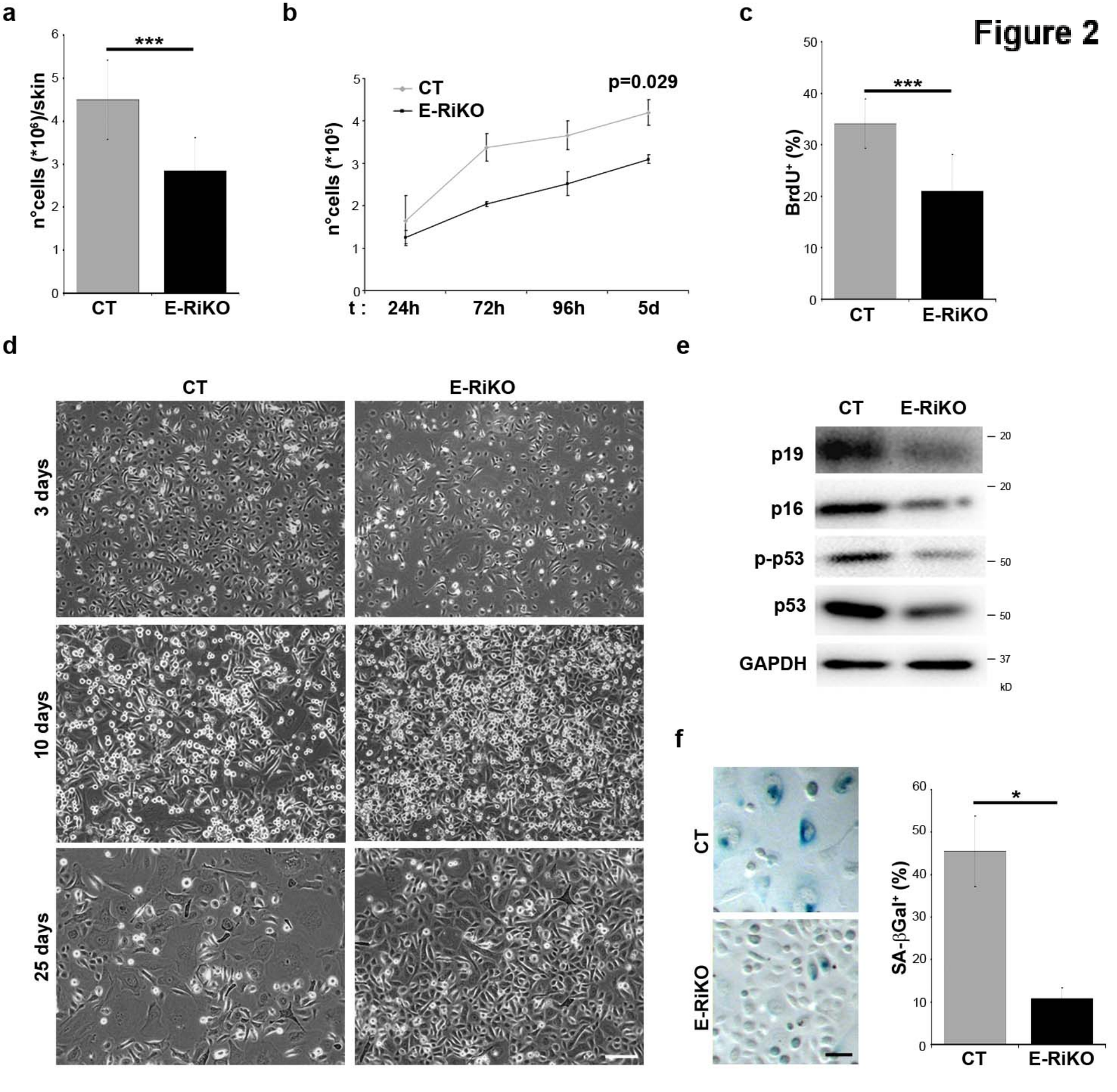
a
***
n°cells (*10⁶)/skin
CT
E-RiKO
b
CT
E-RiKO
p=0.029
n°cells (*10⁵)
t : 24h 72h 96h 5d
c
***
BrdU⁺ (%)
CT
E-RiKO
d
CT
E-RiKO
3 days
10 days
25 days
e
CT
E-RiKO
p19
p16
p-p53
p53
GAPDH
20
20
50
50
37
kD
f
CT
E-RiKO
*
SA-βGal⁺ (%)
CT
E-RiKO

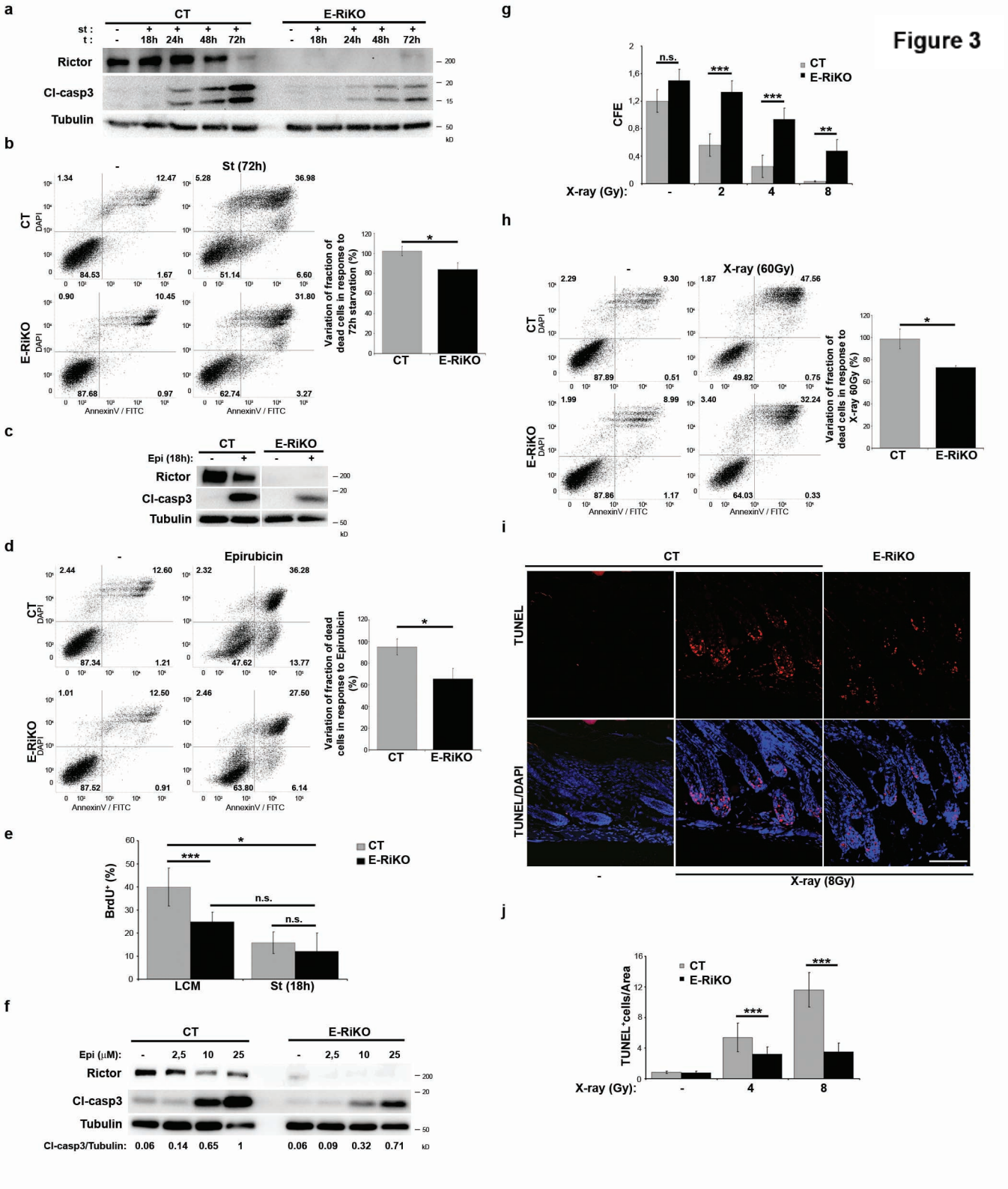
Figure 3
a
CT
E-RiKO
st :
t :
18h
24h
48h
72h
Rictor
Cl-casp3
Tubulin
200
20
15
50
kD
b
St (72h)
CT
E-RiKO
DAPI
AnnexinV / FITC
1.34
12.47
84.53
1.67
5.28
36.98
51.14
6.60
0.90
10.45
87.68
0.97
31.80
62.74
3.27
Variation of fraction of dead cells in response to 72h starvation (%)
c
Epi (18h):
d
Epirubicin
2.44
12.60
87.34
1.21
2.32
36.28
47.62
13.77
1.01
12.50
87.52
0.91
2.46
27.50
63.80
6.14
Variation of fraction of dead cells in response to Epirubicin (%)
e
BrdU⁺ (%)
LCM
St (18h)
n.s.
f
Epi (μM):
Cl-casp3/Tubulin:
0.06
0.14
0.65
1
0.09
0.32
0.71
g
CFE
X-ray (Gy):
h
X-ray (60Gy)
2.29
9.30
87.89
0.51
1.87
47.56
49.82
0.75
1.99
8.99
87.86
1.17
3.40
32.24
64.03
0.33
Variation of fraction of dead cells in response to X-ray 60Gy (%)
i
TUNEL
TUNEL/DAPI
X-ray (8Gy)
j
TUNEL⁺cells/Area

Figure 4

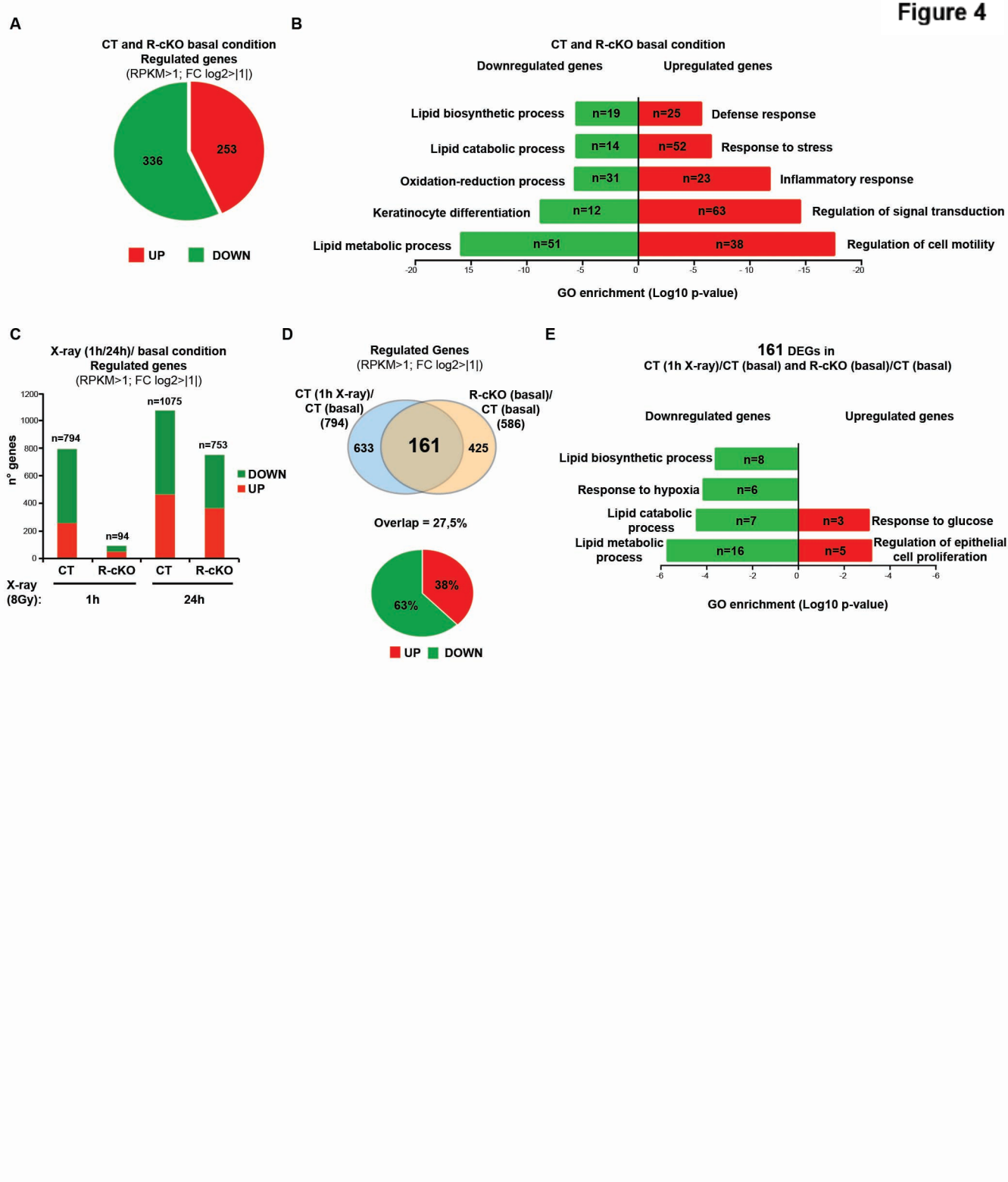
A
CT and R-cKO basal condition
Regulated genes
(RPKM>1; FC log2>|1|)
253
336
UP
DOWN
B
CT and R-cKO basal condition
Downregulated genes
Upregulated genes
Lipid biosynthetic process
n=19
n=25
Defense response
Lipid catabolic process
n=14
n=52
Response to stress
Oxidation-reduction process
n=31
n=23
Inflammatory response
Keratinocyte differentiation
n=12
n=63
Regulation of signal transduction
Lipid metabolic process
n=51
n=38
Regulation of cell motility
-20
15
-10
-5
0
-5
- 10
-15
-20
GO enrichment (Log10 p-value)
C
X-ray (1h/24h)/ basal condition
Regulated genes
(RPKM>1; FC log2>|1|)
n° genes
1200
1000
800
600
400
200
0
n=794
n=94
n=1075
n=753
DOWN
UP
CT
R-cKO
CT
R-cKO
X-ray
(8Gy):
1h
24h
D
Regulated Genes
(RPKM>1; FC log2>|1|)
CT (1h X-ray)/
CT (basal)
(794)
R-cKO (basal)/
CT (basal)
(586)
633
161
425
Overlap = 27,5%
38%
63%
UP
DOWN
E
161 DEGs in
CT (1h X-ray)/CT (basal) and R-cKO (basal)/CT (basal)
Downregulated genes
Upregulated genes
Lipid biosynthetic process
n=8
Response to hypoxia
n=6
Lipid catabolic process
n=7
n=3
Response to glucose
Lipid metabolic process
n=16
n=5
Regulation of epithelial cell proliferation
-6
-4
-2
0
-2
-4
-6
GO enrichment (Log10 p-value)

Figure 5

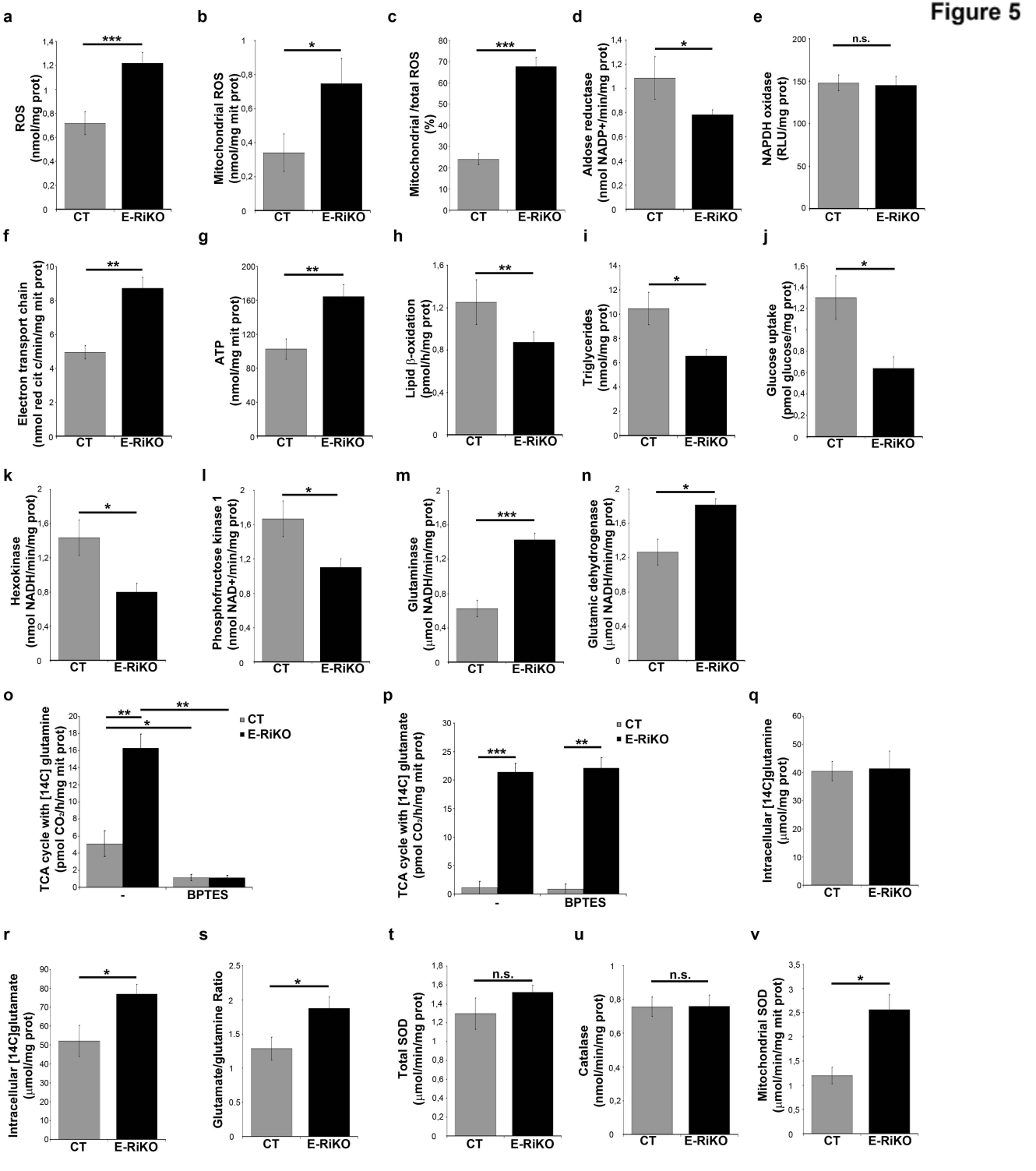
a
ROS (nmol/mg prot)
***
CT
E-RiKO
b
Mitochondrial ROS (nmol/mg mit prot)
*
c
Mitochondrial /total ROS (%)
***
d
Aldose reductase (nmol NADP+/min/mg prot)
*
e
NAPDH oxidase (RLU/mg prot)
n.s.
f
Electron transport chain (nmol red cit c/min/mg mit prot)
**
g
ATP (nmol/mg mit prot)
**
h
Lipid β-oxidation (pmol/h/mg prot)
**
i
Triglycerides (nmol/mg prot)
*
j
Glucose uptake (pmol glucose/mg prot)
*
k
Hexokinase (nmol NADH/min/mg prot)
*
l
Phosphofructose kinase 1 (nmol NAD+/min/mg prot)
*
m
Glutaminase (μmol NADH/min/mg prot)
***
n
Glutamic dehydrogenase (μmol NADH/min/mg prot)
*
o
TCA cycle with [14C] glutamine (pmol CO2/h/mg mit prot)
**
*
**
CT
E-RiKO
-
BPTES
p
TCA cycle with [14C] glutamate (pmol CO2/h/mg mit prot)
***
**
CT
E-RiKO
-
BPTES
q
Intracellular [14C]glutamine (μmol/mg prot)
CT
E-RiKO
r
Intracellular [14C]glutamate (μmol/mg prot)
*
CT
E-RiKO
s
Glutamate/glutamine Ratio
*
CT
E-RiKO
t
Total SOD (μmol/min/mg prot)
n.s.
CT
E-RiKO
u
Catalase (nmol/min/mg prot)
n.s.
CT
E-RiKO
v
Mitochondrial SOD (μmol/min/mg mit prot)
*
CT
E-RiKO

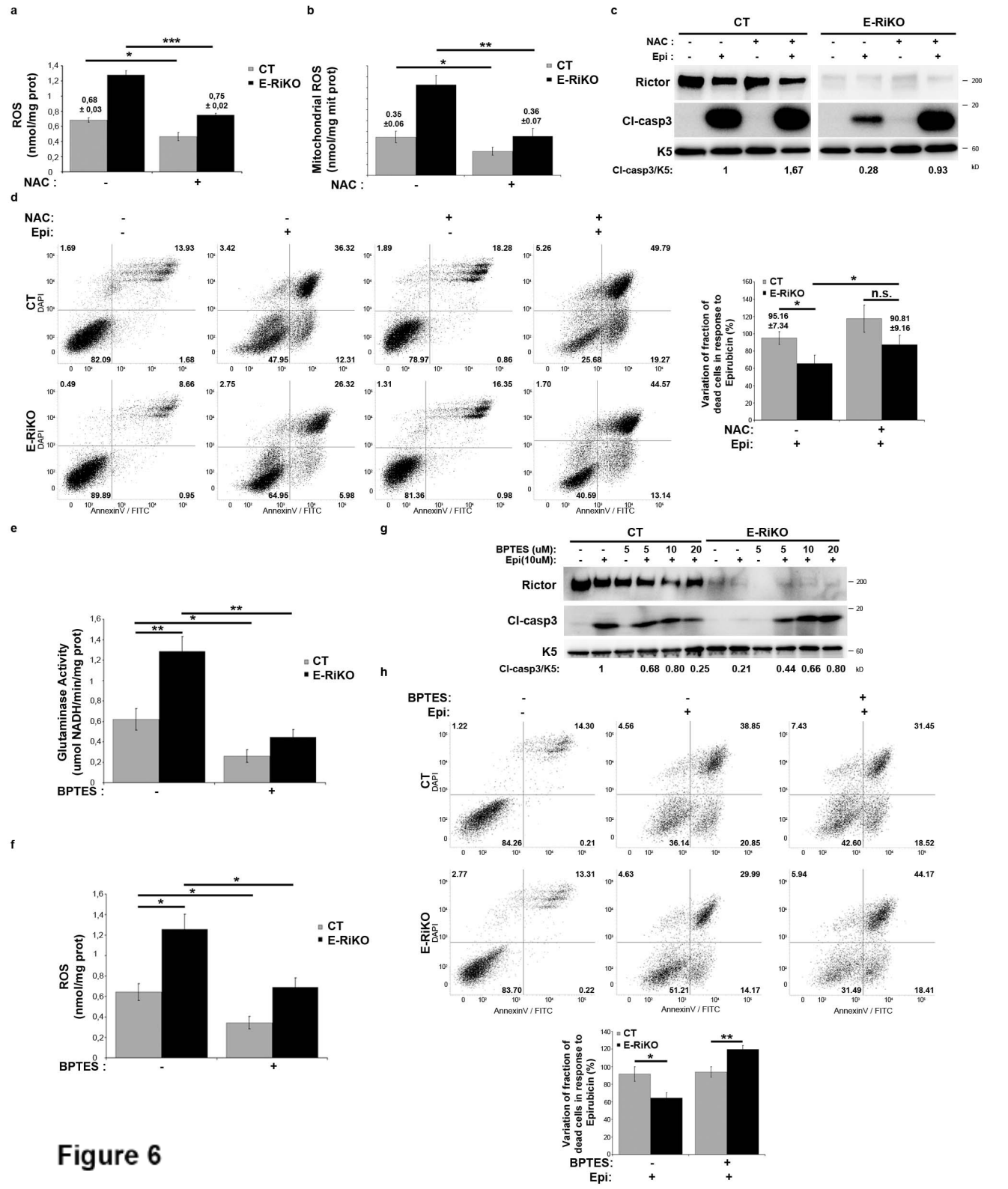
a
ROS (nmol/mg prot)
CT
E-RiKO
0,68 ± 0,03
0,75 ± 0,02
NAC :
b
Mitochondrial ROS (nmol/mg mit prot)
0.35 ±0.06
0.36 ±0.07
c
CT
E-RiKO
Rictor
Cl-casp3
K5
Cl-casp3/K5:
1
1,67
0.28
0.93
kD
d
CT DAPI
E-RiKO DAPI
AnnexinV / FITC
Variation of fraction of dead cells in response to Epirubicin (%)
95.16 ±7.34
90.81 ±9.16
n.s.
e
Glutaminase Activity (umol NADH/min/mg prot)
BPTES :
f
ROS (nmol/mg prot)
g
BPTES (uM):
Epi(10uM):
h
BPTES:
Epi:

Figure 6

Figure 7

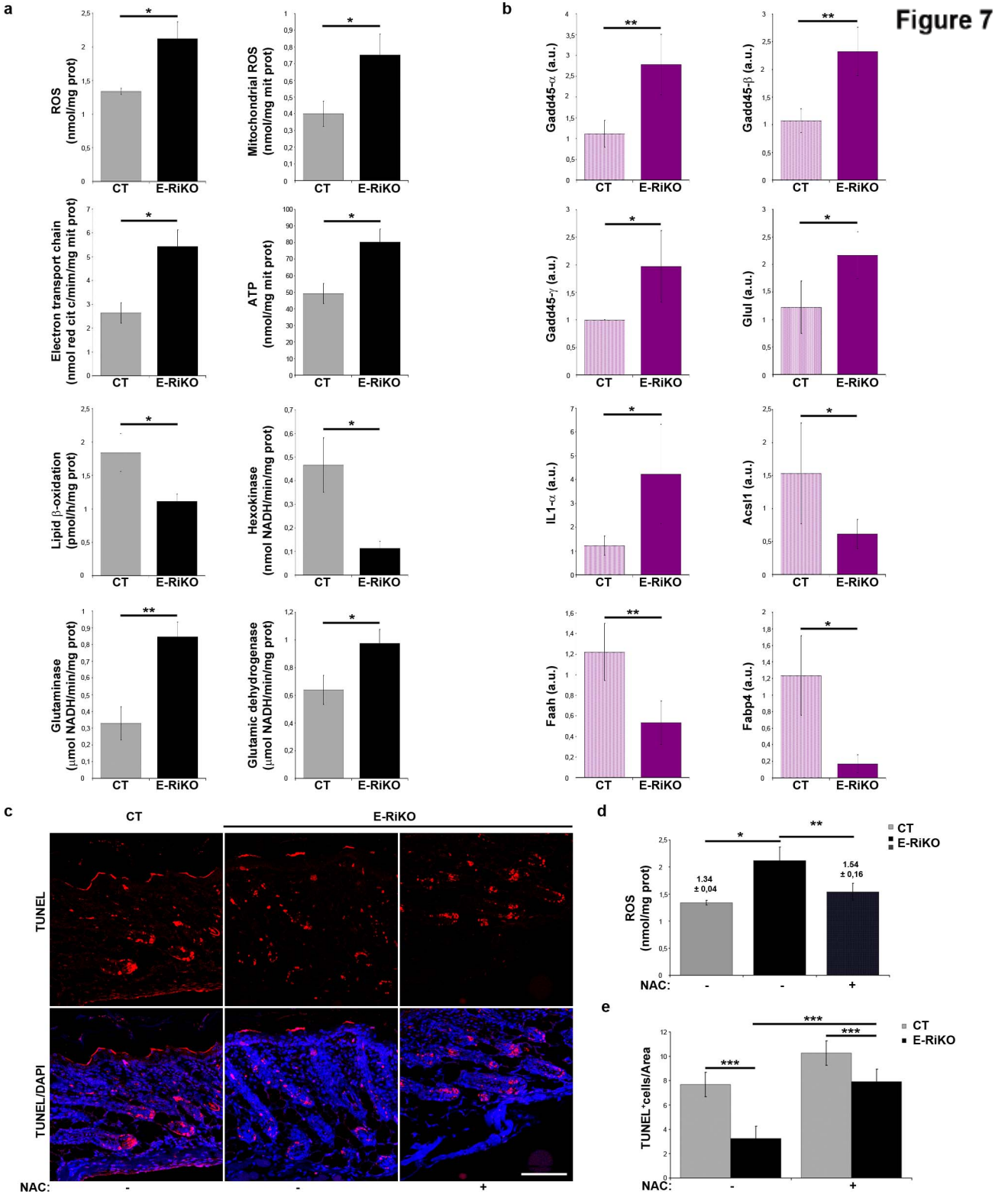
a
ROS (nmol/mg prot)
Mitochondrial ROS (nmol/mg mit prot)
Electron transport chain (nmol red cit c/mim/mg mit prot)
ATP (nmol/mg mit prot)
Lipid β-oxidation (pmol/h/mg prot)
Hexokinase (nmol NADH/min/mg prot)
Glutaminase (μmol NADH/min/mg prot)
Glutamic dehydrogenase (μmol NADH/min/mg prot)
CT
E-RiKO
b
Gadd45-α (a.u.)
Gadd45-β (a.u.)
Gadd45-γ (a.u.)
Glul (a.u.)
IL1-α (a.u.)
Acsl1 (a.u.)
Faah (a.u.)
Fabp4 (a.u.)
c
CT
E-RiKO
TUNEL
TUNEL/DAPI
NAC: - - +
d
ROS (nmol/mg prot)
1.34 ± 0,04
1.54 ± 0,16
NAC: - - +
e
TUNEL+cells/Area
NAC: - +

CDD-16-0309

Title: "Rictor/mTORC2 deficiency enhances keratinocyte stress tolerance via mitohormesis"

1. Supplementary Figure Legends

Figure S1

a) Representative Western blotting analysis on extracts obtained from E-RiKO and CT MPKs treated as in Fig.1c) for the indicated antibodies. b-c) Representative confocal images of IF performed on E-RiKO and CT skin sections as follows: b) with p63 antibody (red) and Dapi (blue). Dotted line: basal lamina. Bar: 25μm. Histograms represent mean ± SD of the percentage of $p63^+$ cells determined on 10 fields of at least 4 mice/genotype. *p<0.05. c) with Loricrin antibody (red) and Dapi (blue). Dotted line: basal lamina. Bar 50μm. Histograms represent mean ± SD of the thickness of Lor^+ layer determined on 10 fields of at least 4 mice/genotype. *p<0.05.

Figure S2

a) BrdU uptake: confluent MPKs, starved for 72h (-) and stimulated with LCM for the indicated times, were supplemented with BrdU for the final 3h. Data are represented as mean ± SD of the percentage of $BrdU^+$ MPKs determined on 200cells/genotype of at least three independent experiments. ***p<0.0005 b) Representative plots of cell cycle analysis by flow cytometry on CT and E-RiKO MPKs maintained for 3 days under proliferating conditions in three independent experiments. Histograms represent mean ± SD of the percentage of cells in each phase of the cell cycle performed on three independent experiments. *p<0.05. c) Diagram of MPKs spontaneous immortalization. Multiple independent CT and E-RiKO cultures were maintained in proliferating conditions until the outgrowth of immortalized

clones that overcame senescence. Confluent clones were trypsinized and subcultured in order to expand selected immortalized clones that are able to support serial passaging in vitro. The experiment was set to passage the selected clones when their cells maintained high cell density for at least one week. The duration of the experiment was approximately 7 months. d) Table of immortalized clones derived from CT and E-RiKO MPKs. Note that in these culture conditions spontaneous immortalization of CT MPKs is a very rare event: 2 clones out of 11 cultures (18%). e) Western blotting analysis for the indicated antibodies of selected immortalized clones (I.clones) derived from E-RiKO and CT MPKs. Note that rictor deletion is maintained upon immortalization in all E-RiKO I.clones.

Figure S3

E-RiKO and CT MPKs were isolated and cultured as in Fig.3. a) Representative phase contrast images of MPKs upon different stressors: Starvation (St), Epirubicin and Cisplatin 5μM for 48h. Bar: 100μm. b) Representative Western blotting analysis for the indicated antibodies of extracts obtained from MPKs maintained in LCM (-) or treated with Cisplatin (5μM) for the indicated times. c) Representative AnnexinV/DAPI flow cytometry plots of E-RiKO and CT MPKs under basal conditions (-) or Cisplatin treatment as in a). Histograms are mean ± SD of dead cells (CT and E-RiKO MPKs) expressed as percentage of variation of dead cells fraction in response to Cisplatin, in three independent experiments. d) Representative Western blotting analysis for the indicated antibodies of extracts obtained from CT and E-RiKO MPKs maintained in LCM (-) or treated with X-ray (8Gy) for the indicated times. e) Representative images of X-ray treated MPKs with the indicated doses, stained for SA-βGal (upper panel). The percentage of SA-βGal^{+} cells is quantified in the histograms (lower panel) as mean ± SD of at least 200 cells/genotype of three independent experiments. Bar: 100μm. ***$p<0.0005$. f) Total cellular ROS was measured upon LCM (-) or X-ray treatment (8Gy) for

24h. Histograms represent mean ± SD of ROS levels measured in at least three independent experiments. ***p<0.0005; **p<0.005; *p<0.05.

Figure S4

a) Glutaminase activity (μmol NADH/min/mg prot) was measured upon LCM (-) or BPTES treatment. Histograms represent mean ± SD of Glutaminase activity levels measured in at least three independent experiments. **p<0.005; *p<0.05. b) Representative Western blotting analysis on extracts obtained from CT and E-RiKO MPKs under proliferative conditions, with the indicated antibodies.

Figure S5

a) Representative Western blotting analysis of extracts obtained from CT MPKs kept in LCM (-) or NAC 10mM for 24h and treated or not (-) with Epirubicin at the indicated doses for 10h, with the indicated antibodies. b) Histograms represent mean ± SD of total cellular ROS in E-RiKO and CT MPKs maintained in LCM (-) or treated with NAC 10mM for 24h of at least three independent experiments. **p<0.005; ***p<0.0005. c) Representative Western blotting analysis of extracts obtained from CT MPKs maintained under proliferative conditions and E-RiKO cells treated with Trolox at the indicated doses for 48h and subsequently treated or not (-) with Epirubicin for 10h, with the indicated antibodies. d) Histograms represent mean ± SD of total cellular ROS in E-RiKO and CT MPKs maintained in LCM (-) or treated with Trolox 1mM for 48h of at least three independent experiments. *p<0.05. e) E-RiKO and CT MPKs were maintained in LCM (-) or treated with NAC 10mM for 48h and analysed for the following metabolic parameters: Electron transport chain (nmol red cit c/min/mg mit prot); ATP (nmol/mg mit prot); Hexokinase (nmol NADH/min/mg prot); Lipid β-oxidation (pmol/h/mg prot); Glutaminase (μmol NADH/min/mg prot); Glutamic dehydrogenase (μmol NADH/min/mg prot); Catalase

(nmol/min/mg prot); Total SOD (μmol/min/mg prot); Mitochondrial SOD (μmol/min/mg prot).All histograms represent mean ± SD of the indicated metabolic parameters determined in at least three independent experiments. **p<0.005; *p<0.05.

Figure S6

Original Western blotting images are reported.

Figure S7

Original Western blotting images are reported.

2. Supplementary Table Legends

Table S1

RNA-seq: List of genes expressed in CT and E-RiKO MPKs analyzed as in Fig.4. Number of reads is represented as RPKM.

Table S2

List of upregulated genes in E-RiKO vs CT under basal conditions.

Table S3

List of downregulated genes in E-RiKO vs CT under basal conditions.

Table S4

List of GO enrichments from the list of upregulated genes in E-RiKO vs CT under basal conditions. GO with a nominal p value<10^{-3} were considered.

Table S5

List of GO enrichments from the list of downregulated genes in E-RiKO vs CT under basal conditions. GO with a nominal p value<10^{-3} were considered.

Table S6

List of GO enrichments relative to the list of upregulated genes in the overlapping 161DEGs as in Fig. 4d). GO with a nominal p value<10^{-3} were considered.

Table S7

List of GO enrichments relative to the list of downregulated genes in the overlapping 161DEGs as in Fig. 4d). GO with a nominal p value<10^{-3} were considered.

Figure S1

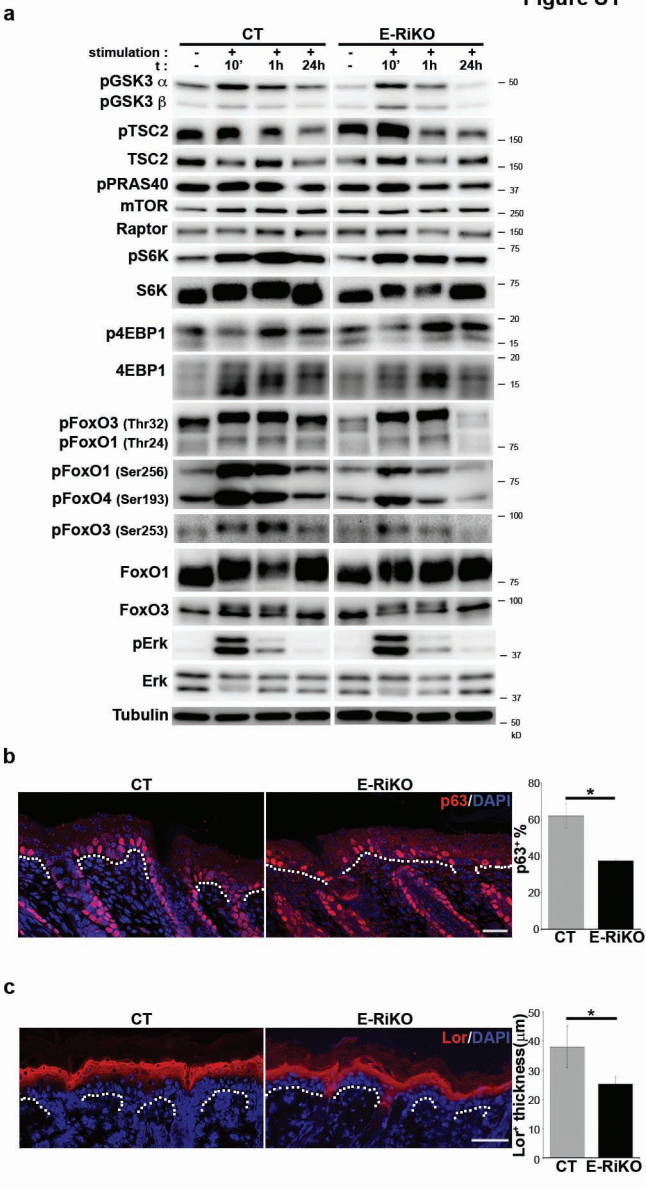
a
CT
E-RiKO
stimulation :
t :
- + + +
- 10' 1h 24h
pGSK3 α
pGSK3 β
pTSC2
TSC2
pPRAS40
mTOR
Raptor
pS6K
S6K
p4EBP1
4EBP1
pFoxO3 (Thr32)
pFoxO1 (Thr24)
pFoxO1 (Ser256)
pFoxO4 (Ser193)
pFoxO3 (Ser253)
FoxO1
FoxO3
pErk
Erk
Tubulin
50
150
150
37
250
150
75
75
20
15
20
15
75
75
100
75
100
37
37
50
kD
b
CT
E-RiKO
p63/DAPI
p63+%
80
60
40
20
0
*
CT
E-RiKO
c
CT
E-RiKO
Lor/DAPI
Lor thickness(μm)
50
40
30
20
10
0
*
CT
E-RiKO

Figure S2

a

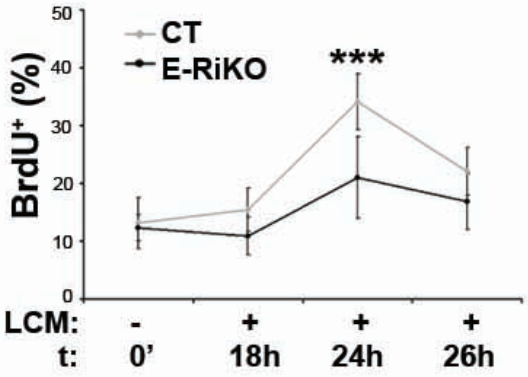

b

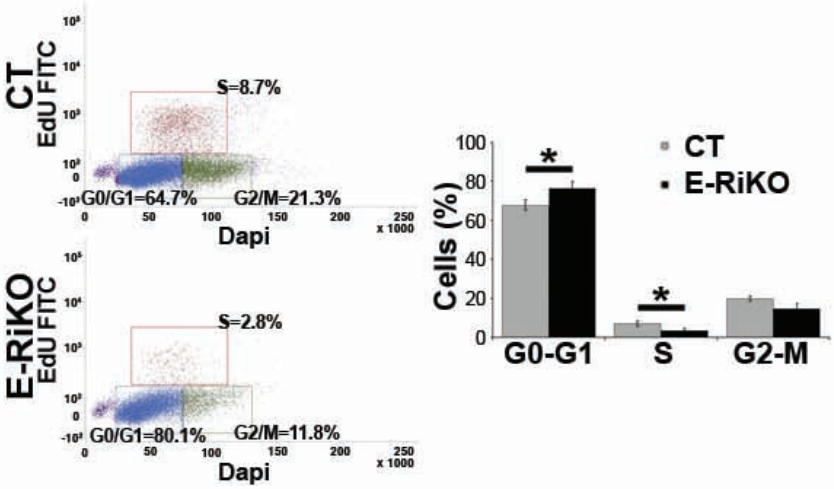

c

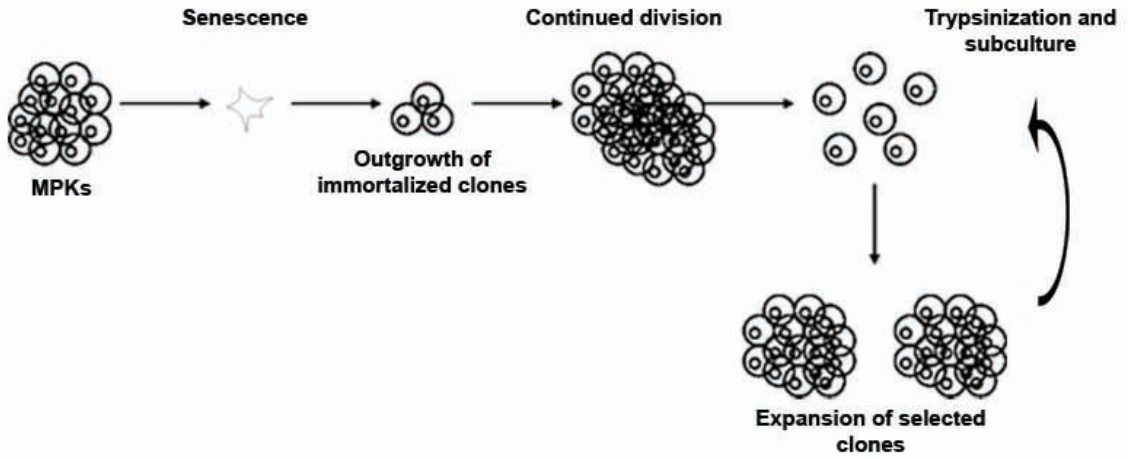

d

MPKs	n° samples	Immortalized clones	%
CT	11	2	18
E-RiKO	7	7	100

e

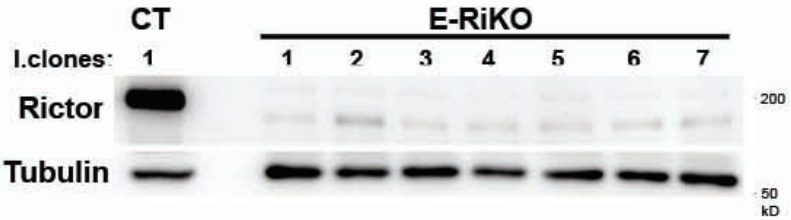

Figure S3

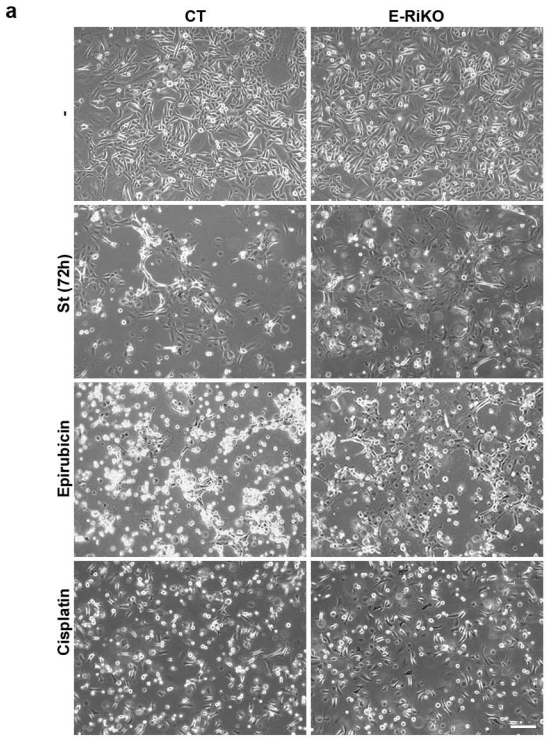
a
CT
E-RiKO
-
St (72h)
Epirubicin
Cisplatin

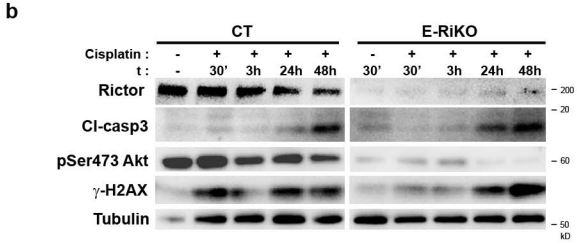
b
CT
E-RiKO
Cisplatin :
t :
Rictor
Cl-casp3
pSer473 Akt
γ-H2AX
Tubulin
kD

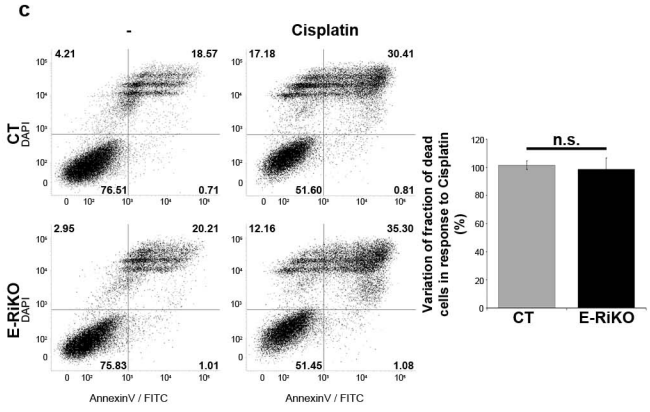
c
-
Cisplatin
CT
E-RiKO
DAPI
AnnexinV / FITC
Variation of fraction of dead cells in response to Cisplatin (%)
n.s.

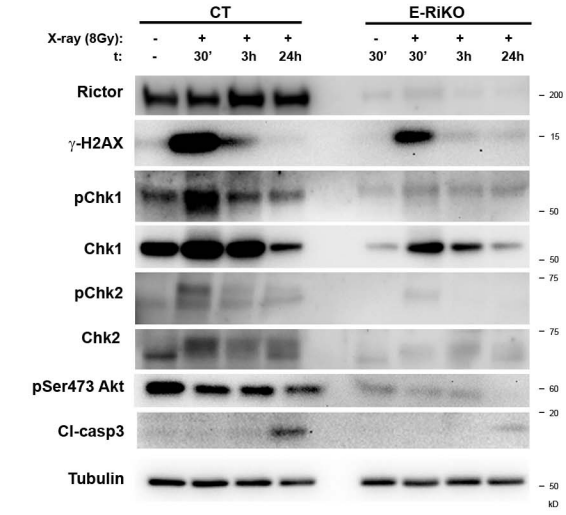
d
CT
E-RiKO
X-ray (8Gy):
t:
Rictor
γ-H2AX
pChk1
Chk1
pChk2
Chk2
pSer473 Akt
Cl-casp3
Tubulin
kD

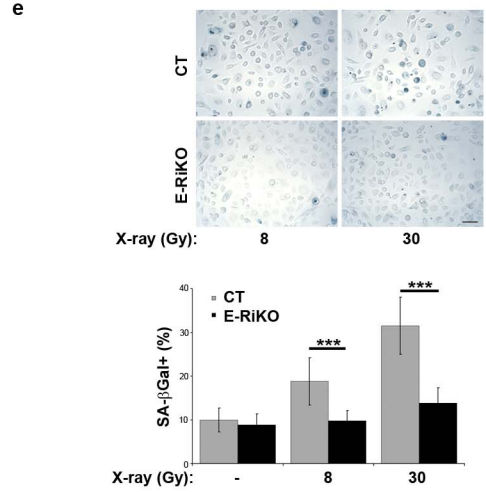
e
CT
E-RiKO
X-ray (Gy):
SA-βGal+ (%)
***

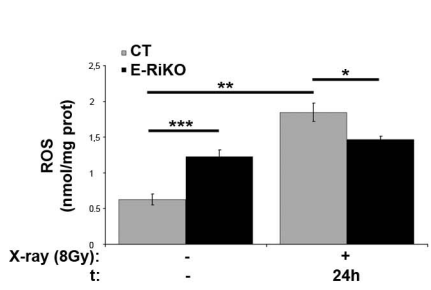
f
CT
E-RiKO
ROS (nmol/mg prot)
*
**
***
X-ray (8Gy):
t:

Figure S4

a

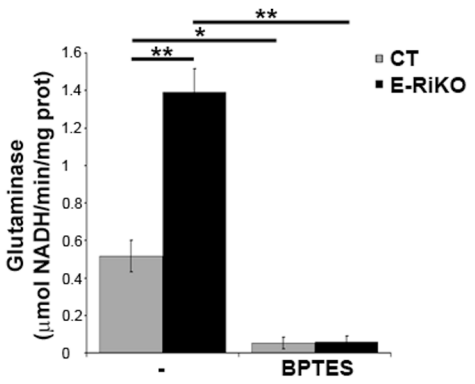
**
*
**
CT
E-RiKO
Glutaminase
(µmol NADH/min/mg prot)
1.6
1.4
1.2
1
0.8
0.6
0.4
0.2
0
-
BPTES

b

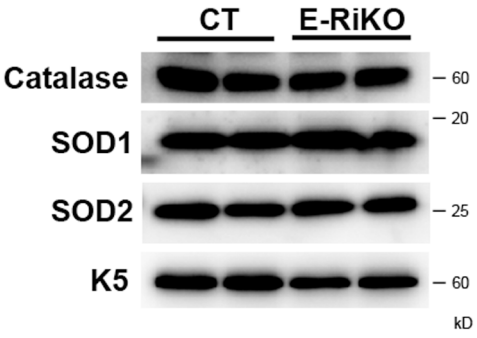
CT
E-RiKO
Catalase
SOD1
SOD2
K5
60
20
25
60
kD

Figure S5

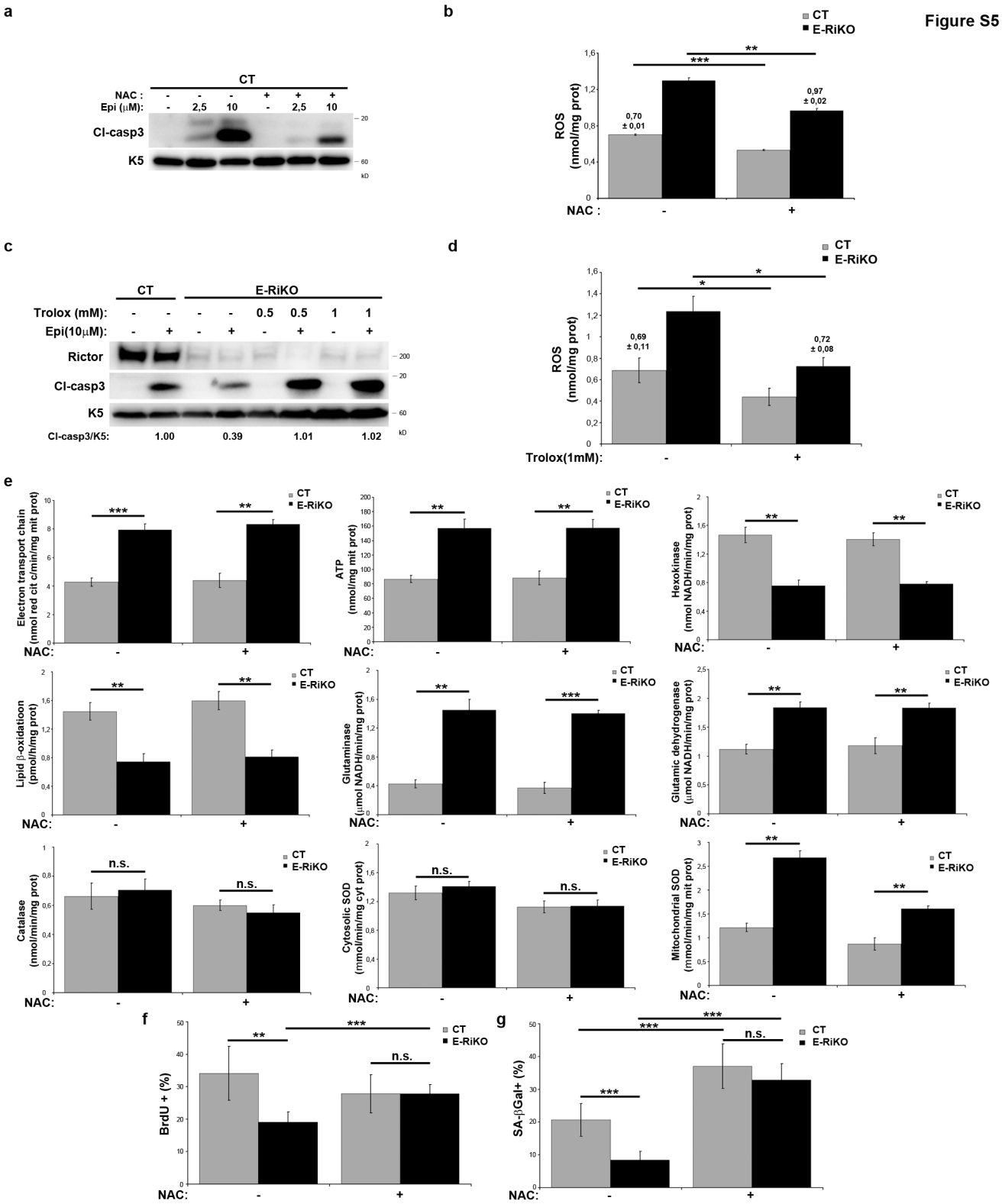
a
CT
NAC : - - - + + +
Epi (μM): - 2,5 10 - 2,5 10
Cl-casp3
K5
20
60
kD
b
CT
E-RiKO
ROS (nmol/mg prot)
0,70 ± 0,01
0,97 ± 0,02
NAC : - +
c
CT
E-RiKO
Trolox (mM): - - - - 0.5 0.5 1 1
Epi(10μM): - + - + - + - +
Rictor
Cl-casp3
K5
200
20
60
kD
Cl-casp3/K5: 1.00 0.39 1.01 1.02
d
CT
E-RiKO
ROS (nmol/mg prot)
0,69 ± 0,11
0,72 ± 0,08
Trolox(1mM): - +
e
Electron transport chain (nmol red cit c/min/mg mit prot)
ATP (nmol/mg mit prot)
Hexokinase (nmol NADH/min/mg prot)
Lipid β-oxidatioon (pmol/h/mg prot)
Glutaminase (μmol NADH/min/mg prot)
Glutamic dehydrogenase (μmol NADH/min/mg prot)
Catalase (nmol/min/mg prot)
Cytosolic SOD (mmol/min/mg cyt prot)
Mitochondrial SOD (mmol/min/mg mit prot)
n.s.
NAC: - +
f
BrdU + (%)
NAC: - +
g
SA-βGal+ (%)
NAC: - +

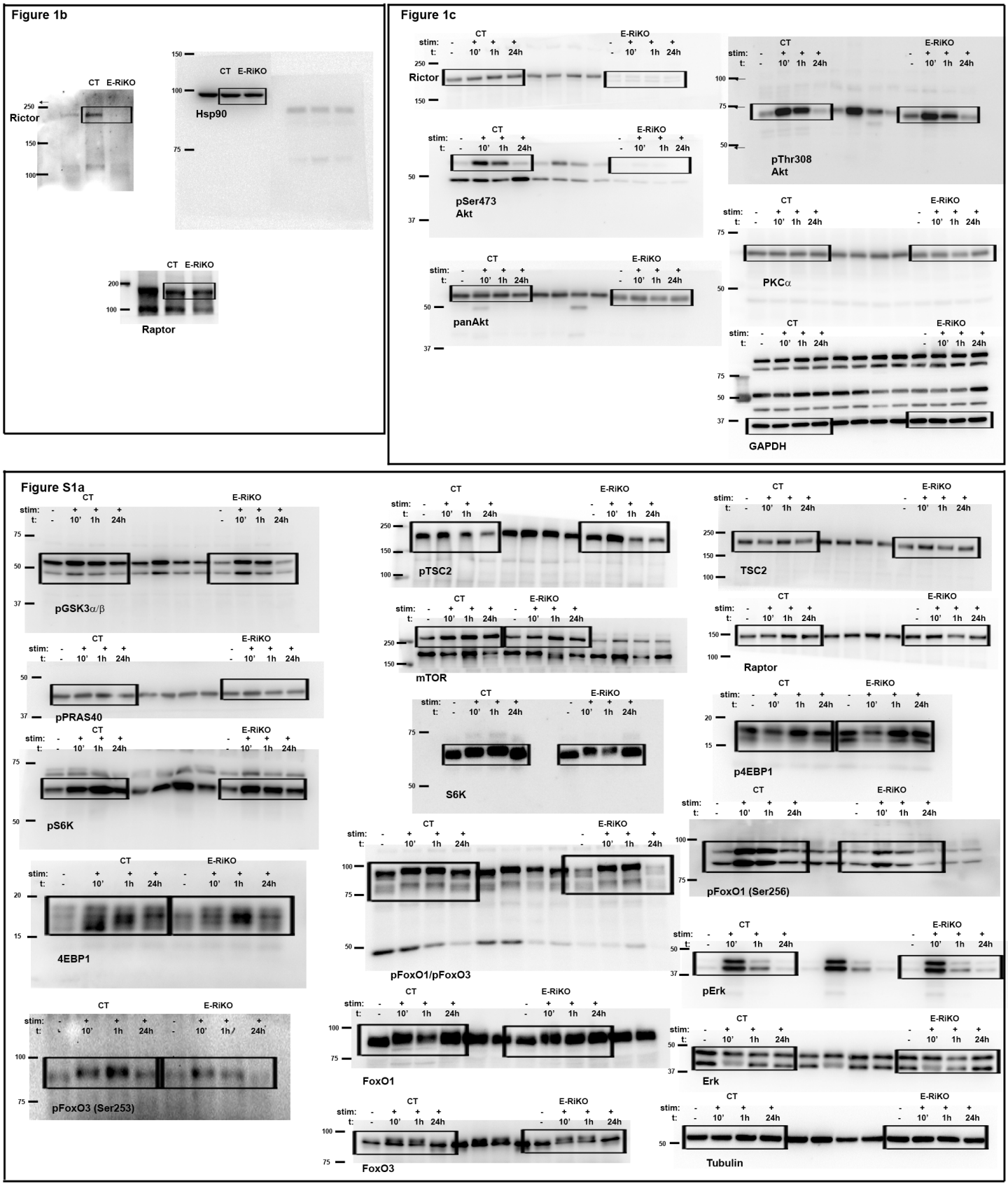
Figure 1b
CT E-RiKO
Rictor
250
150
100
CT E-RiKO
Hsp90
150
100
75
CT E-RiKO
Raptor
200
100
Figure 1c
CT E-RiKO
stim: - + + + - + + +
t: - 10' 1h 24h - 10' 1h 24h
Rictor
250
150
pSer473 Akt
50
37
panAkt
50
37
pThr308 Akt
100
75
50
PKCα
75
50
GAPDH
75
50
37
Figure S1a
pGSK3α/β
75
50
37
pPRAS40
50
37
pS6K
75
50
4EBP1
20
15
pFoxO3 (Ser253)
100
75
pTSC2
250
150
100
mTOR
250
150
S6K
75
50
pFoxO1/pFoxO3
100
75
50
FoxO1
100
75
FoxO3
100
75
TSC2
250
150
100
Raptor
150
100
p4EBP1
20
15
pFoxO1 (Ser256)
100
75
pErk
50
37
Erk
50
37
Tubulin
50

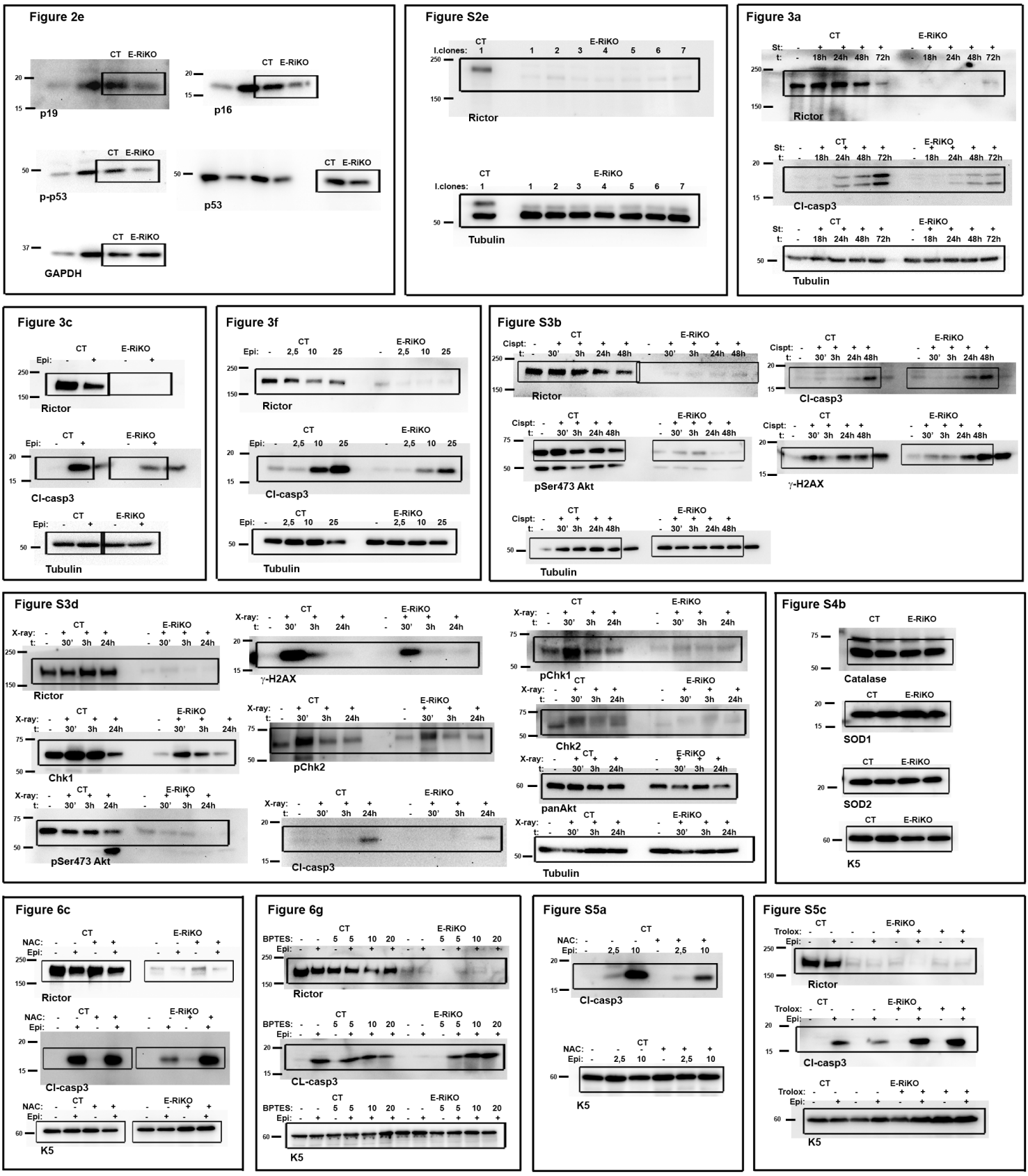
Figure 2e
CT E-RiKO
p19
p16
p-p53
p53
GAPDH
Figure S2e
l.clones: 1 1 2 3 4 5 6 7
Rictor
Tubulin
Figure 3a
St: - + + + + - + + + +
t: - 18h 24h 48h 72h - 18h 24h 48h 72h
Rictor
Cl-casp3
Tubulin
Figure 3c
Epi: - + - +
Rictor
Cl-casp3
Tubulin
Figure 3f
Epi: - 2,5 10 25 - 2,5 10 25
Rictor
Cl-casp3
Tubulin
Figure S3b
Cispt: - + + + + - + + + +
t: - 30' 3h 24h 48h - 30' 3h 24h 48h
Rictor
Cl-casp3
pSer473 Akt
γ-H2AX
Tubulin
Figure S3d
X-ray: - + + + - + + +
t: - 30' 3h 24h - 30' 3h 24h
Rictor
γ-H2AX
Chk1
pChk2
pSer473 Akt
Cl-casp3
pChk1
Chk2
panAkt
Tubulin
Figure S4b
Catalase
SOD1
SOD2
K5
Figure 6c
NAC: - - + + - - + +
Epi: - + - + - + - +
Rictor
Cl-casp3
K5
Figure 6g
BPTES: - - 5 5 10 20 - - 5 5 10 20
Epi: - + - + + + - + - + + +
Rictor
CL-casp3
K5
Figure S5a
NAC: - - - + + +
Epi: - 2,5 10 - 2,5 10
Cl-casp3
K5
Figure S5c
Trolox: - - - - + + + +
Epi: - + - + - + - +
Rictor
Cl-casp3
K5